Check for updates

Nonlinear dynamic analysis and experimental study of multi-link press with dry friction clearances of revolute joints

Xiulong Chen · Jingqing Wang

Abstract In mechanical system, the clearance between revolute joints is ineluctable, which will influence the motion precision and constancy of the system. Currently, studies of simple mechanisms with single clearance are relatively mature, but in-depth studies of sophisticated mechanisms with several clearances are not enough. For the purpose of investigating non-linear dynamic properties of multiple clearances and multi-degree of freedom complex mechanisms, a nonlinear dynamic analysis framework of multi-link mechanism with dry friction clearances was proposed, the rigid body dynamic model of planar 7-bar mechanism containing dry friction clearances was built and analyzed in this paper. To analyze effects of clearances on dynamic response of the mechanism, taking a seven-bar press with mixed driven as an illustration, a dynamic modeling and analytical technique of press mechanism containing dry friction clearances was proposed. Firstly, the clearance model was established according to relevant geometrical relations, then contact force model and friction model were established. Furthermore, Lagrange multiplier method was adopted to set up the rigid body dynamics equation which would be solved by Runge–Kutta method. Secondly, influences of different factors on dynamic response were studied, and correctness of model was verified by emulation contrast with ADAMS. Thirdly, non-linear properties of mechanism were analyzed by related images. Finally, the experimental platform of seven-bar mechanism was built to check the validity of outcomes. The researches provided a foundation for prediction of dynamic trajectory of press mechanism in theory, and settled a solid basis for excogitation and fabrication of high-accuracy press mechanism.

1 Introduction

In actual production, as a result of existence of machining accuracy, friction, wear, and so on, clearances in kinematic joints are unavoidable. Clearances could reduce machining accuracy, decrease the service life of mechanical systems and even damage parts. For example, in the polishing process of large-sized ceramic slabs [1] by a polishing machine, there will be clearances of the revolute joints between the grinding plate and the frame, which will reduce the polishing accuracy of ceramic slabs to a certain extent. Planar linkage is more common in press mechanism, with universality and generality. While the study of dynamic response and nonlinear

X. Chen (✉) · J. Wang
College of Mechanical and Electronic Engineering,
Shandong University of Science and Technology,
Qingdao 266590, China
e-mail: cxldy99@163.com

characteristics can intuitively show the influence of kinematic joint clearances on mechanical system. Therefore, it is of vital essentiality to conduct modeling and analysis of planar linkage mechanism with dry friction clearances and to investigate effect of clearances on its dynamic response and nonlinear properties.

Currently, numbers of researchers have made much progress when modeling and analyzing simple mechanical constructs containing single clearance. However, there are few studies relatively on multi-clearance complex mechanisms. Ma et al. [2] put forward a modeling method for contact force model of complex contact surfaces. Chen, Feng et al. [3] carried out dynamic modeling and dynamic characteristics analysis of crank-slider mechanical constructs with clearances. In optimizing the connecting bar length, centroid position and other parameters of planar linkage mechanism, Etesami et al. [4] used multi-objective inheritance method of calculation. Bai et al. [5, 6] put forward an optimization technique for bad oscillation due to clearances on connecting bar mechanism. Subsequently, they improved the configuration of biaxial driven mechanism of satellite antenna with double revolute joint clearances. Erkaya [7] studied the effect of bulbar articulations with clearances and flexible junctures on mechanism oscillation through experiments. Chen, Zhang et al. [8] built rock-cracking mechanism model of plane multi-clearance joints and performed dynamic resolution. Chen et al. [9] conducted rigid body dynamics modeling and analysis of planar 9-bar mechanism containing clearances. Marques et al. [10] considered effects of chafe modeling in dynamic response of multi-body systems. To calculate abrasion of low-speed revolute joints of multi-link mechanisms, Lai et al. [11] raised an efficacious technique. Oruganti et al. [12] researched oscillation and impact phenomena of multi-clearance systems by experimental and computational methods. Ambrosio et al. [13] proposed an integrate formula for clearance modeling of kinematic articulation in several frame systems. Taking 4-bar mechanisms containing two clearances of revolute joints as an example, Tan et al. [14] proposed a consecutive researching technique for multi-body dynamics system. Song, Yang et al. [15] took planar shunt connection mechanisms as an example to analyze coupling effect of articulations with clearances and flexible links in the parallel mechanism. Ebrahimi et al. [16] analyzed

effects of clearances on vibration factors with regard to instantaneous natural frequency and mode of vibration of flexible four-bar mechanism. Wang et al. [17] raised frictional contact without penetrating analysis method with regard to crank slider mechanism as an example.

At the same time, many scholars have made innovative breakthroughs in the analysis of dynamic response of several connecting bars mechanisms containing single clearance. However, analysis of dynamic response as well as non-linear properties of complicated mechanisms with several clearances is relatively few. Chen et al. [18] analyzed dynamic characteristics of multi-clearance planar 4-bar mechanisms containing flexible links. Erkaya [19] researched effects of clearances of kinematic joints with regard to power consumption of main actuator of mechanical system of three-dimensional crank slider mechanisms. Jiang and Chen [20] analyzed effects of different clearance sizes as well as driving speeds with regard to composite clearances mechanism through experiments. Chen et al. [21] studied influences of different clearances and friction models with regard to dynamic properties of two dimensions mechanisms. Li, Wang et al. [22] studied dynamic characteristics of two dimensions inflexible-flexible coherent solar battery aligned system with clearances of kinematic joint. Tan et al. [23] studied dynamic properties of a planar mechanism containing clearances on account of contact force model together with LuGre friction model. To carry out dynamic analysis of two dimensions mechanisms containing several clearances of revolute joints, isometric analysis method was adopted by Pi et al. [24]. Tan et al. [25] analyzed effects of friction on dynamic properties of 4-bar mechanisms with two dimensions containing clearance joints. Bai et al. [26] studied effects of mechanism flexibility on dynamic properties of a 4-bar mechanism with clearances. Li et al. [27] took planar deployable structures of shear elements on this account to analyze influences of revolute joint clearances at distinct positions on their dynamic behaviors. Varedi-koulaei et al. [28] analyzed effects of clearances of kinematic pair with regard to dynamics of 3RRR parallel robot with two dimensions. To assess non-linear properties of multi-body mechanisms, Chen et al. [29] proposed a synthetical method. Wu, Sun et al. [30] analyzed system confusions problem of planar multi-clearance 4-bar mechanisms. Liu et al. [31] studied bifurcation phenomenon of periodic motion of a 3-DOF vibration-impact system containing

clearances. Kong, Tian et al. [32] raised comprehensive calculation techniques to study nonlinear sloshing dynamics of liquid-filled space satellite system under microgravity acceleration. Yousuf [33] studied the nonlinear deed of multi-wheel cam driven link configurations through experiments and simulations.

Based on the above analysis, rare studies have been done on complicated mechanisms containing several clearances, the researches with regard to dynamic response and non-linear properties of complicated planar mechanisms containing several clearances are also even less. At the same time, the researches on the mechanism with clearances are mostly concentrated in theory, while the relevant experimental researches are less. Therefore, for the purpose of analyzing dynamic response and nonlinear properties of mechanisms containing dry friction clearances and researching effects of clearances with regard to mechanical system, a nonlinear dynamic analysis framework combining theory with experiment was proposed. the article adopted 7-bar mechanisms as an illustration to conduct a thorough research. The structure of this article is as below. For Sect. 2, on account of L-N model together with improved Coulomb friction force model, contact force model in normal direction as well as friction force model in tangent direction of rotational joint clearances was built separately. For Sect. 3, with regard to Lagrange multiplier technique, dynamic model of 7-bar mechanisms containing clearances was established. With respect to Sect. 4, the influences of clearance, friction coefficient and driving speed on dynamic response of press were analyzed respectively. Furthermore, correctness of model is verified by simulation comparison between MATLAB and ADAMS. In Sect. 5, the effects concerning clearance values as well as driving velocity on the non-linear properties of press mechanism were analyzed via using associated analysis graph. In Sect. 6, experimental platform of seven-bar mechanism was built, and validity of results in theory was proved through tests.

2 Development of clearance model

2.1 Construction of the revolute clearance model

The vector model with regard to clearances is signified as Fig. 1. OXY is global coordinate of the system. $o_i x_i y_i$ and $o_j x_j y_j$ are local coordinate system of bearing and shaft respectively. o_i and o_j are centroids of bearing together with shaft separately. M_i as well as M_j is centers of bearing and shaft.

The eccentric vector of bearing together with shaft is

$$e = r_j^M - r_i^M \tag{1}$$

The unit vector of the eccentric vector is

$$n = \frac{e}{e} \tag{2}$$

Among them, $e = \sqrt{e^{\mathrm{T}} e}$.

When the bearing and the shaft collide, the collision depth is

$$\delta = e - r \tag{3}$$

where r refers to clearance value, $r = R_i - R_j$. R_i as well as R_j is radius of bearing and shaft separately.

As is shown in Fig. 2, the corresponding motion state of bearing and shaft could be divided into unrestrained condition, successive contact condition and collision condition.

Three kinds of motion states between revolute joint elements can be judged by the depth of collision.

When $\delta < 0$, there is no collision between bearing and shaft;

When $\delta = 0$, bearing and shaft are in collision or separation state;

When $\delta > 0$, a collision occurs between the bearing and the shaft.

The collision occurs between t_n and t_{n+1}, which can be expressed as

$$\delta(t_n)\delta(t_{n+1}) < 0 \tag{4}$$

While the collision takes place, position vector of collision point of shaft together with bearing is expressed as

$$\begin{cases} r_i^N = r_i^M + R_i n \\ r_j^N = r_j^M + R_j n \end{cases} \tag{5}$$

First-order differentiation of formula (5) concerning time can be obtained, and the velocity vector of collision point is

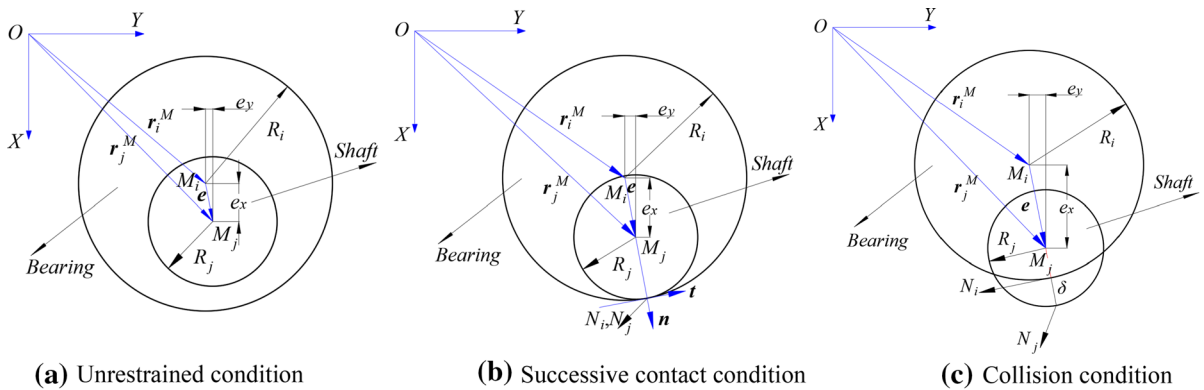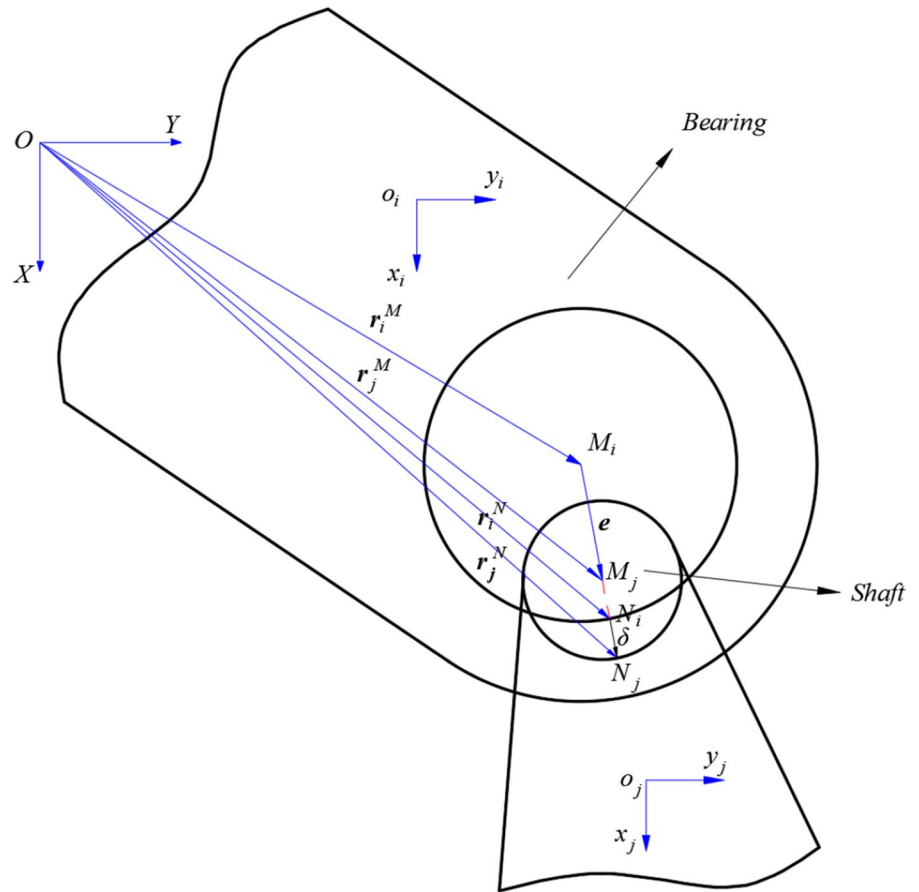**Fig. 1** Vector model with regard to revolute joint clearances

(a) Unrestrained condition   **(b)** Successive contact condition   **(c)** Collision condition

Fig. 2 Relative motion of elements in revolute joints

$$\begin{cases} \dot{r}_i^N = \dot{r}_i^M + R_i \dot{n} \\ \dot{r}_j^N = \dot{r}_j^M + R_j \dot{n} \end{cases} \qquad (6)$$

The velocity vector of collision point is projected to two orientations perpendicular to each other of this plane where the collision occurs, and relative speeds are

$$\begin{cases} v_n = \left(\dot{r}_j^N - \dot{r}_i^N \right)^T n \\ v_t = \left(\dot{r}_j^N - \dot{r}_i^N \right)^T t \end{cases} \tag{7}$$

2.2 Development of the normal contact force model

Lots of scholars have conducted numbers of analyses of collision problems and discussed different collision force models. In the article, improved Hertz model was applied to establish normal contact force model, which considered energy loss, material characteristics and partly elastic deformation generated by collision. According to the literature [3, 15], its expression is

$$F_n = K\delta^n + D\dot{\delta} \tag{8}$$

where, F_n is contact force of normal orientation; $\dot{\delta}$ is relative penetration speed; n is the compensation factor, and the value depends on features of material; K is stiffness coefficient; D is damping coefficient.

According to the literature [6], stiffness coefficient K is expressed as

$$K = \frac{4}{3\left(\delta_i + \delta_j\right)} \sqrt{\frac{R_i R_j}{R_i - R_j}} \tag{9}$$

where, $\delta_k = \frac{1-\mu_k^2}{E_k} (k = i, j)$; E_k is elastic modulus of bearing together with shaft; μ_k is the Poisson's proportion with regard to the bearing as well as shaft.

According to the literature [8], the damping coefficient D is expressed as

$$D = \frac{3K\left(1 - c_e^2\right)\delta^n}{4\dot{\delta}^{(-)}} \tag{10}$$

Among this, c_e is recovery parameter; $\dot{\delta}^{(-)}$ is primary collision speed.

2.3 Improvement of the tangent friction force model

Coulomb friction model is usually applied for considering friction caused by revolute joints. In Coulomb friction model, friction force is positively correlated with normal tension. At the same time, orientation of friction force is opposite to relative slipping speed. For the purpose of computing figure

constancy, Ambrósio raised an advanced friction model based on primary Coulomb friction model to calculate numerical constancy. According to the literature [5, 23], the modified Coulomb friction is shown in following formula.

$$F_t = -c_f c_d F_n \frac{v_t}{|v_t|} \tag{11}$$

Among this, c_f is friction coefficient; v_t is corresponding slipping speed; c_d is motional revised coefficient and according to the literature [14], its expression is

$$c_d = \begin{cases} 0 & , |v_t| < v_0 \\ \dfrac{|v_t| - v_0}{v_1 - v_0}, v_0 \leq |v_t| \leq v_1 \\ 1 & , |v_t| > v_1 \end{cases} \tag{12}$$

where, v_0 as well as v_1 is limit values of quiescent friction and dynamic friction velocities respectively.

Through analyzing above contact force of normal orientation and tangential friction model, resultant collision force with dry friction clearance could be obtained.

$$F_{dry} = F_n n + F_t t \tag{13}$$

The force and torque equivalent to the bearing centroid are

$$F_{ij} = F_n n + F_t t = \begin{bmatrix} F_{ij}^x & F_{ij}^y \end{bmatrix}^T \tag{14}$$

$$M_{ij} = -\left(y_i^N - y_i\right)F_{ij}^x + \left(x_i^N - x_i\right)F_{ij}^y \tag{15}$$

where, F_{ij}^x and F_{ij}^y represent the components of collision forces in X and Y directions.

Forces as well as moments effective to center of mass of axis are

$$F_{ji} = -F_{ij} \tag{16}$$

$$M_{ji} = -\left(y_j^N - y_j\right)F_{ji}^x + \left(x_j^N - x_j\right)F_{ji}^y \tag{17}$$

3 Dynamics modeling of seven-bar mechanism concerning clearances

3.1 The constructive properties concerning the mechanism

Structure diagram concerning seven-bar mechanism is represented as Fig. 3. It contains a rack, driving crank 1 and 4, connecting link 2, connecting link 3, connecting link 6 and slider 7. Clearance A is situated at revolute joints with regard to driving crank 1 together with link 2, similarly clearance B is situated at revolute joints with regard to driving crank 4 together with link 3. Due to the clearance at the crank has a great influence on the mechanism, position A

and B located at two cranks are adopted for analysis. There are two DOF with regard to this mechanism. To ensure a firm movement of this mechanism, a mixed driven type is selected. In other words, driving crank 1 is operated through dc motor, while driving crank 4 is operated via servo device. Advantage of mixed operation is that mechanism can achieve several different trajectories, and can meet the requirements of different pressure machining processes. The mechanism is widely used in low-speed and heavy-duty mechanical systems and precision instruments.

Fig. 3 Schematic diagram of structure of hybrid driven seven bar press
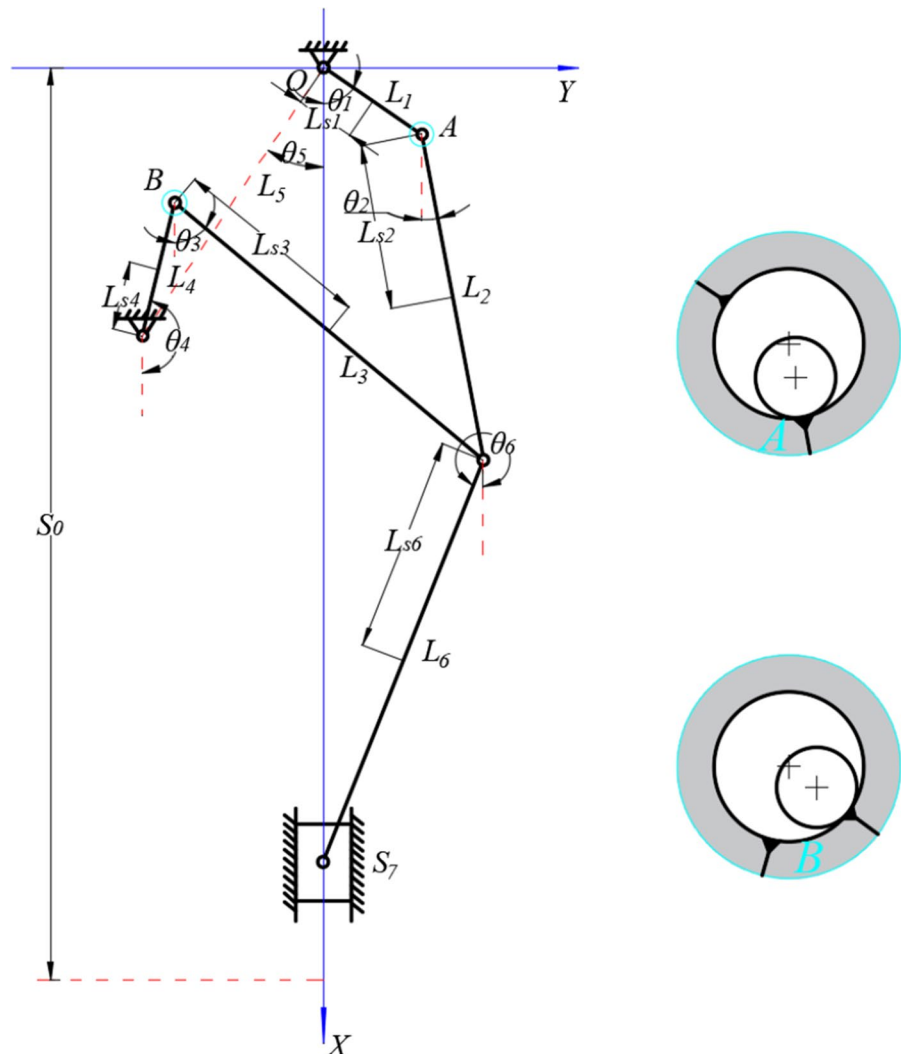
3.2 Establishment of dynamic model

According to Fig. 3, the corresponding global generalized coordinates are as follows.

$$q_i = \begin{pmatrix} x_i & y_i & \theta_i \end{pmatrix}^T \quad (i = 1, 2, 3, 4, 6, 7) \tag{18}$$

Among this, x_i together with y_i is component with regard to structural member i in X and Y orientations in axes of whole situation. In addition, θ_i is revolute angle concerning i relative to positive direction of X-axis.

Therefore, the generalized coordinates of planar seven-bar mechanism are

$$q = \begin{pmatrix} x_1 \ y_1 \ \theta_1 \ x_2 \ y_2 \ \theta_2 \ x_3 \ y_3 \ \theta_3 \\ x_4 \ y_4 \ \theta_4 \ x_6 \ y_6 \ \theta_6 \ x_7 \ y_7 \ \theta_7 \end{pmatrix} \tag{19}$$

Each planar kinematic joint will introduce two constraints. Ideally, a 7-bar mechanism in a plane possesses 6 rotational joints, 1 translational joint together with 2 driving restrictions, and 18 restrictive equations could be produced. At the same time, the clearances are taken into account at rotational joint A along with B, and constraint equations of 2 kinematic joints are reduced by 4. Therefore, restrictive equations of 7-bar mechanism in a plane containing double clearances are

$$\Phi(q, t) = \begin{vmatrix} x_1 - L_{s1} \cos \theta_1 \\ y_1 - L_{s1} \sin \theta_1 \\ x_2 + L_{s2} \cos \theta_2 - x_3 - L_{s3} \cos \theta_3 \\ y_2 + L_{s2} \sin \theta_2 - y_3 - L_{s3} \sin \theta_3 \\ x_4 - L_{s4} \cos \theta_4 - L_5 \cos \theta_5 \\ y_4 - L_{s4} \sin \theta_4 - L_5 \sin \theta_5 \\ x_2 + L_{s2} \cos \theta_2 - x_6 + L_{s6} \cos \theta_6 \\ y_2 + L_{s2} \sin \theta_2 - y_6 + L_{s6} \sin \theta_6 \\ x_6 + L_{s6} \cos \theta_6 - x_7 \\ y_6 + L_{s6} \sin \theta_6 - y_7 \\ y_7 \\ \theta_7 - 180^\circ \\ \theta_1 - \omega_1 t \\ \theta_4 - 216.46^\circ - \omega_4 t \end{vmatrix} = 0 \tag{20}$$

First-order differentiation of formula (20) is taken concerning time, and velocity constraint equation is achieved.

$$\Phi_q \dot{q} = -\Phi_t \equiv \upsilon \tag{21}$$

Φ_q is Jacobian matrix with regard to restrictive equations, and it is obtained by taking partial derivatives of the constraint equation to generalized coordinates, $\Phi_q = \frac{\partial \Phi}{\partial q}$; Φ_t is partial differentiation with regard to constraint equation concerning time, $\Phi_t = \frac{\partial \Phi}{\partial t}$; $\dot{q}$ is general speed vector.

The second differentiation of formula (20) concerning time is obtained, and restrictive equation of accelerated speed is

$$\Phi_q \ddot{q} = -\left(\Phi_q \dot{q}\right)_q \dot{q} - 2\Phi_{qt} \dot{q} - \Phi_{tt} \equiv \gamma \tag{22}$$

where, $\ddot{q}$ is generalized acceleration vector; Φ_{qt} is partial derivative of Jacobian matrix concerning time; Φ_{tt} is second partial derivative of restrictive equation concerning time.

Rigid body dynamics equation relatively is established based on Lagrange multiplier method.

$$M\ddot{q} + \Phi_q^T \lambda = g \tag{23}$$

Among this, M is mass matrix concerning system, λ is Lagrange multiplicator, in addition, g is general force with regard to system.

Mass matrix of system could be shown as

$$M = diag\begin{pmatrix} m_1 \ m_1 \ J_1 \ m_2 \ m_2 \ J_2 \ m_3 \ m_3 \ J_3 \\ m_4 \ m_4 \ J_4 \ m_6 \ m_6 \ J_6 \ m_7 \ m_7 \ J_7 \end{pmatrix} \tag{24}$$

where m_i is mass concerning member i while J_i is rotational inertia with regard to member i.

On the basis of formulas (22) along with (23), rigid body dynamics formula of mechanism is

$$\begin{pmatrix} M & \Phi_q^T \\ \Phi_q & 0 \end{pmatrix} \begin{pmatrix} \ddot{q} \\ \lambda \end{pmatrix} = \begin{pmatrix} g \\ \gamma \end{pmatrix} \tag{25}$$

Equation (25) can be used to calculate $\ddot{q}$ and λ. However, kinematic displacement constraints and velocity constraints are not be introduced in Eq. (25), which could produce a default problem when solving equation. According to the literature [20], Baumgarte raised a default stabilization algorithm to solve the default problem by applying this two constraints to accelerated speed constraint equation.

$$\begin{pmatrix} M & \Phi_q^T \\ \Phi_q & 0 \end{pmatrix} \begin{pmatrix} \ddot{q} \\ \lambda \end{pmatrix} = \begin{pmatrix} g \\ \gamma - 2\alpha\dot{\Phi} - \beta^2\Phi \end{pmatrix} \qquad (26)$$

where α and β are correction coefficients, $\alpha > 0, \beta > 0$, $\dot{\Phi} = \frac{d\Phi}{dt}$.

4 Analysis of dynamic response concerning seven-bar mechanism with dry friction clearances

4.1 Solution flow chart

The Runge–Kutta technique was applied for analyzing the rigid body dynamical equation with regard to multi-link mechanism containing dry friction clearances. The flowsheet is revealed as Fig. 4, and the specific flow is as follows:

(1) The initial conditions, structural parameters, geometric parameters and clearance parameters of the planar seven-bar mechanism were defined;

(2) The clearance model was built to judge collision state and analyze normal and tangent force when collision occurred;

(3) The mass matrix, Jacobian matrix as well as general force were calculated, while dynamics equation concerning the seven-bar mechanism with dry friction clearance was established;

(4) A default stability algorithm was proposed based on Baumgarte. The Runge–Kutta technique was applied for analyzing the dynamics equation with regard to a planar 7-bar mechanical stucture containing dry friction clearance, while generalized

coordinates, generalized velocities and generalized accelerations were obtained;

(5) Repeat the above process until the final solution time is reached.

4.2 System data

Geometric data concerning planar seven-bar mechanism were shown as Table 1, structural data with regard to planar seven-bar mechanism were shown as Table 2, and clearance parameters with respect to the revolute joints were shown as Table 3.

4.3 Dynamic response

4.3.1 Effects concerning clearance value with regard to dynamic response

This chapter analyzes effects of distinct clearance figures on dynamic response with regard to the rigid body seven-bar mechanism containing dry friction clearance, and considers that there are clearances at both A and B of the revolute joints. The clearance figures at A as well as B of the revolute joint are all 0.1 mm, 0.3 mm and 0.5 mm, and compared with the ideal situation. The friction coefficient was selected as 0.01, and driving velocity of crank 1 together with crank 4 was $\omega_1 = \pi$rad/s and $\omega_4 = -\pi$rad/s accordingly. The displacement, velocity as well as acceleration of the slider 7 are revealed as Fig. 5, and collision force and collision track at the clearances of the revolute joints are revealed as Fig. 6 to Fig. 7.

Fig. 4 Flow chart of solving rigid body dynamical equation with regard to multi-link mechanism containing dry friction clearances
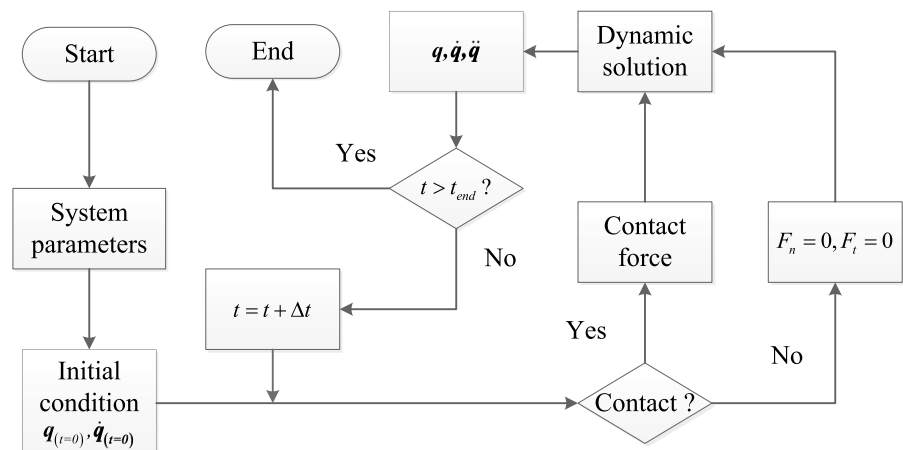
Table 1 Geometric data

Parameter	Parameter values	Parameter	Parameter values
Length of crank 1 L_1/(m)	0.161089	Center of mass distance of crank 4 L_{s4}/(m)	0.057083
Center of mass distance of crank 1 L_{s1}/(m)	0.0805445	Distance of two fixed hinge L_5/(m)	0.509678
Length of Connecting link 2 L_2/(m)	0.674046	The angle between the two fixed hinges and the x axis θ_5/(°)	−40.392
Center of mass distance of Connecting link 2 L_{s2}/(m)	0.337023	Length of connecting link 6 L_6/(m)	1.114569
Length of connecting link 3 L_3/(m)	0.669907	Center of mass distance of connecting link 6 L_{s6}/(m)	0.5572845
Center of mass distance of connecting link 3 L_{s3}/(m)	0.3349535	Distance between the origin of coordinates and the lower limit of the slider S_0/(m)	1.949704
Length of crank 4 L_4/(m)	0.114166		

Table 2 The structural parameters

Parameter	Parameter values	Parameter	Parameter values
Mass of crank 1 m_1/(kg)	0.1900300161	Moment of inertia of crank 1 J_1/(kg m²)	$4.2632877711 \times 10^{-4}$
Mass of connecting link 3 m_2/(kg)	0.7902666497	Moment of inertia of connecting link 2 J_2/(kg m²)	0.030072948456
Mass of connecting link 3 m_3/(kg)	0.7854233988	Moment of inertia of connecting link 3 J_3/(kg m²)	0.02952384924
Mass of crank 4 m_4/(kg)	0.1351230677	Moment of inertia of crank 1 J_4/(kg m²)	$1.5634512491 \times 10^{-4}$
Mass of connecting link 6 m_6/(kg)	1.3057446381	Moment of inertia of connecting link 6 J_6/(kg m²)	0.135550343
Mass of slider 7 m_7/(kg)	0.023126858927	Moment of inertia of slider 7 J_7/(kg m²)	$1.6780635677 \times 10^{-6}$

Table 3 Clearance parameters of revolute joints

Parameter	Parameter values
Radius of bearing R_i/(m)	0.015
Coefficient of restitution c_e	0.9
Modulus of elasticity E_i, E_j/(GPa)	200
Poisson's ratio μ_i, μ_j	0.3
Correction coefficient of normal contact force model n	1.5
Baumgarte's correction coefficient α, β	50
Integral step (s)	0.0001

In Fig. 5a, the displacement summits of ideal condition, 0.1 mm clearance, 0.3 mm clearance and 0.5 mm clearance are 528.1 mm, 527.9 mm, 527.6 mm and 527.1 mm respectively, indicating that in the wake of rise of clearance figure, displacement peak value of sliding block 7 decreases slightly, but in general, clearance value has little effects with regard to displacement of slider 7. As is shown in Fig. 5b, the bigger clearance value is, the larger sawtooth swings concerning the speed image is, especially

at initial position. For Fig. 5c, acceleration image vibrates sharply before 0.4 s, then the vibration attenuation tends to be stable, which is basically consistent with the ideal situation. The peak acceleration at 0.1 mm, 0.3 mm and 0.5 mm clearance values reach 149.4 m/s², 270.7 m/s² and 592.9 m/s² respectively, indicating the bigger clearance figure is, the bigger the peak value with regard to acceleration fluctuation is, at the same time, the more severe the impact on the mechanism is.

In Fig. 6a, the collision force of revolute joint A at 0.1 mm clearance, 0.3 mm clearance and 0.5 mm clearance reaches its peak value of 415.5 N at 0.0046 s, 741.6 N at 0.0076 s, 1569 N at 0.0238 s. According to Fig. 6b, while clearance figures are 0.1 mm, 0.3 mm and 0.5 mm, peak figures of the collision force at position B take place at 0.008 s, 0.0408 s, and 0.0856 s, and figures are 328.2 N, 597.6 N and 705.8 N respectively, indicating that the collision force at clearances increases in the wake of rise of clearance value. In case of the equivalent clearance figure, collision force at location A is larger than that at location B, suggesting the revolute joint

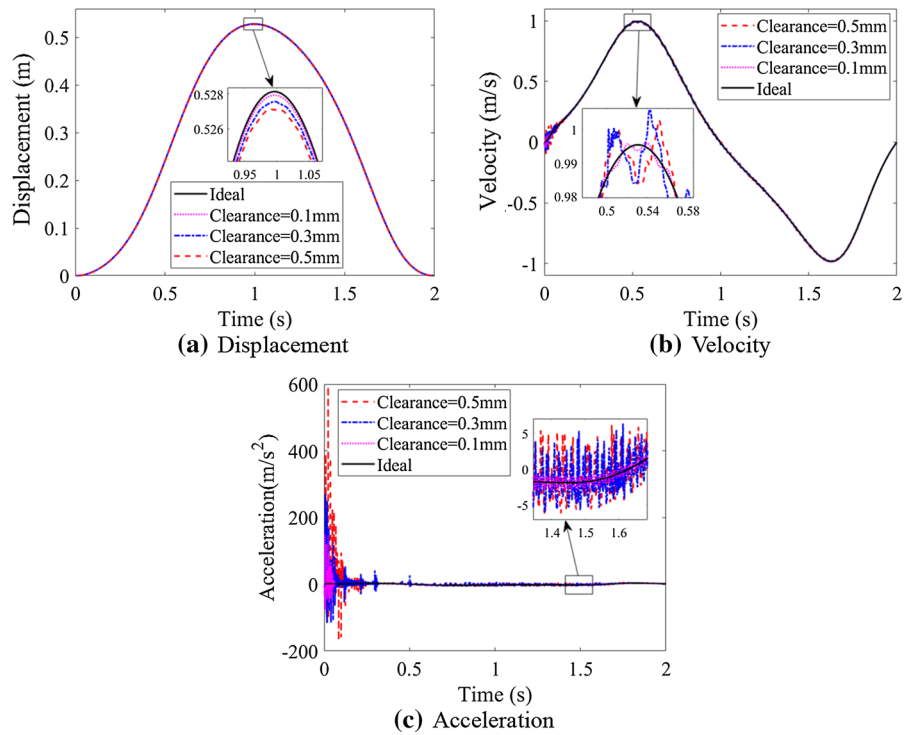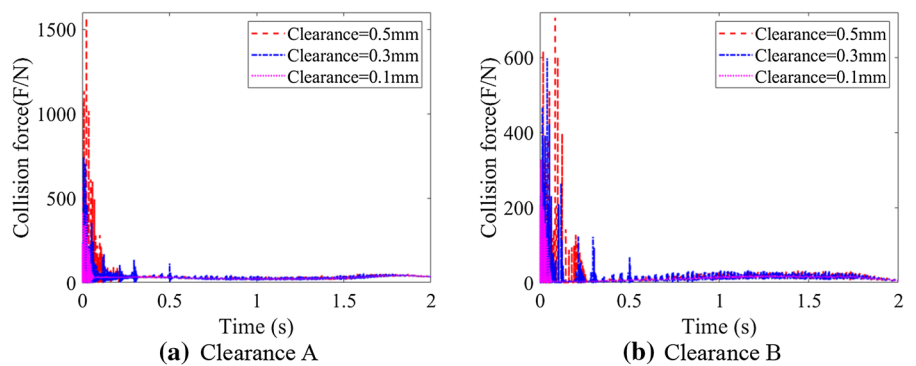**Fig. 5** Dynamic response
of mechanism

(a) Displacement

(b) Velocity

(c) Acceleration

Fig. 6 Collision force at
clearances

(a) Clearance A

(b) Clearance B

clearance A has stronger influences on the mechanism than that at location B.

Figure 7a, b are the collision track images at A and B of the revolute joint clearance respectively. The collision trajectories at the clearance B of the revolute joints are more chaotic than those at clearance A of the revolute joints. Simultaneously, with the increase of clearance value, motion range at clearance A as well as clearance B gets larger, indicating that rise with regard to clearance figure makes central trajectory at the clearances more complex. Furthermore, the

relative contact concerning shafts along with bearings increases, which emerges greater effects concerning constancy for mechanism.

4.3.2 *Effects of friction coefficient in relation to dynamic response*

The part analyzes influence of different friction coefficients with respect to dynamic response of planar 7-bar mechanism with dry friction clearance, and

(a) Clearance A
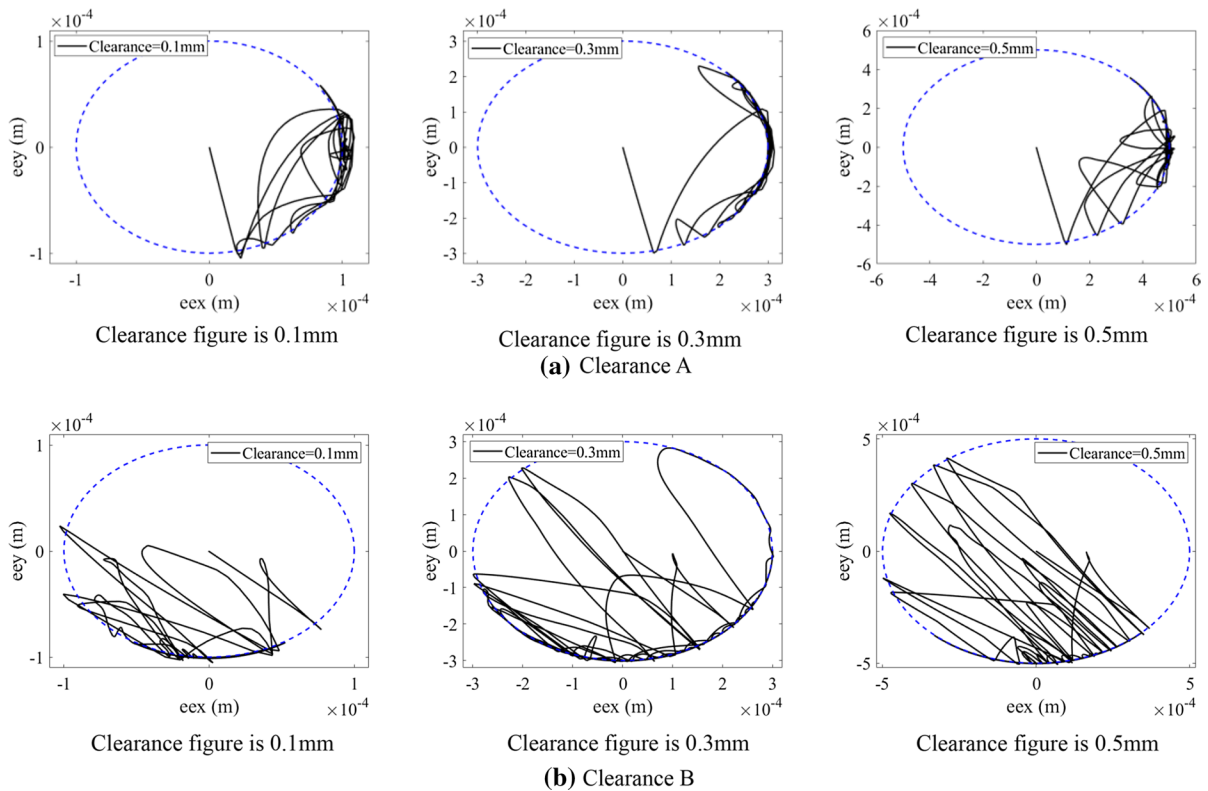
(b) Clearance B

Fig. 7 Collision trajectory of shaft

considers that there are clearances at both A and B of the revolute joints. The friction coefficients concerning 0.01, 0.05 and 0.1 were selected as comparative researches with ideal condition. Clearance values at both A and B of the revolute joints were selected for 0.5 mm, and driving speeds of driving crank 1 and 4 were $\omega_1 = \pi$rad/s along with $\omega_4 = -\pi$rad/s respectively. The displacement, speed as well as acceleration of slider 7 are shown as Fig. 8, concurrently, collision force and collision track at the clearances are revealed as Fig. 9 together with Fig. 10.

In Fig. 8a, displacement curves with friction coefficients of 0.01, 0.05 and 0.1 almost coincide, and the peak value is slightly lower than the ideal condition, indicating change of friction coefficient has mild effects concerning displacement of slider, and dry friction clearance will slightly reduce the peak value of displacement. According to the speed image in Fig. 8b, the velocity fluctuation range generated while friction coefficient is 0.01 is the most extensive, indicating that the more minor friction coefficient is, the greater volatility with respect to velocity curve is. In

Fig. 8c acceleration comparison diagram, during the period of 0~0.3 s, the image vibrates violently. While friction coefficients are 0.01, 0.05 and 0.1, summits about acceleration take place at 0.0238 s, 0.0096 s and 0.0098 s separately, and summits are 592.9 m/s², 374.7 m/s² and 334.5 m/s² respectively, indicating that while friction modulus increases at the range of 0.01 to 0.1, summits of acceleration decreases and the amplitude of the vibration decreases.

Figure 9 reveals collision force images at A and B of the revolute joint clearances. Collision force at two revolute joint clearances generates high peak values and violent vibration before 0.3 s, and the vibration weakens significantly and tends to be stable after 0.3 s. In Fig. 9a, while friction coefficients are 0.01, 0.05 and 0.1, summits of collision force at location A occurs at 0.0238 s, 0.0096 s and 0.0098 s separately, and peak value is 1569 N, 1020 N and 901.4 N respectively. In Fig. 9b, while friction coefficients are 0.01, 0.05 and 0.1, summits of collision force at location B occurs at 0.0856 s, 0.0238 s and 0.0146 s, and the peak value is 705.8 N, 739.9 N

Fig. 8 Dynamic response of mechanism

(a) Displacement

(b) Velocity

(c) Acceleration

Fig. 9 Collision force at clearance
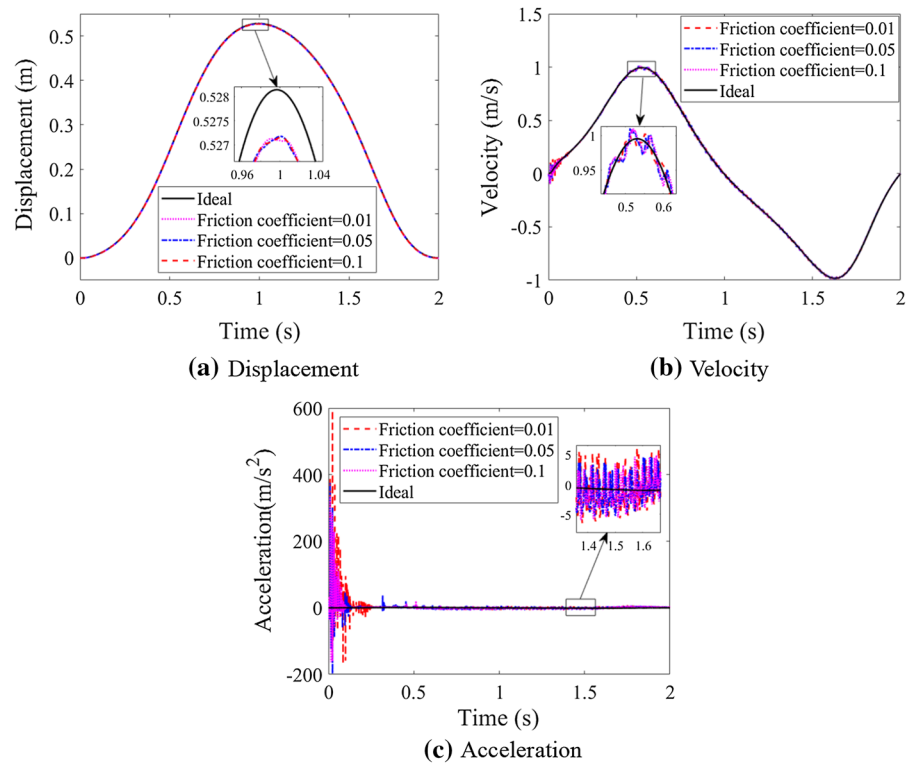
(a) Clearance A
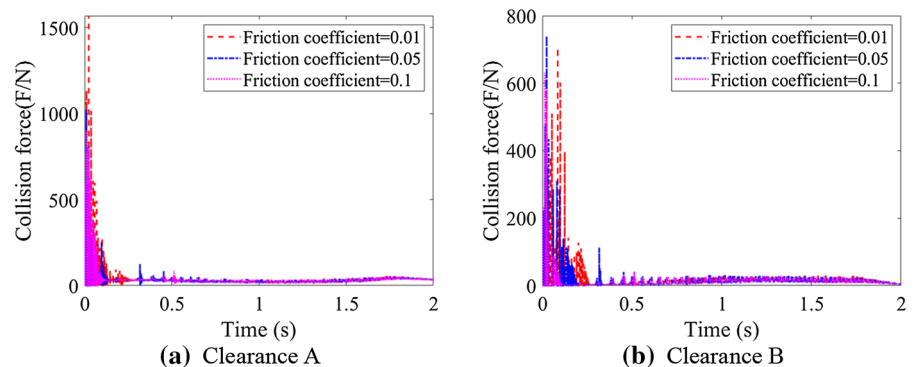
(b) Clearance B

and 631 N respectively. This shows that in the wake of rise of friction coefficient, oscillation frequency with regard to collision force at clearances decreases and the peak value decreases relatively. However, the collision force at location A is larger than that at location B, manifesting the clearance at location A has momentous effects with respect to mechanism than that at location B.

According to the images of collision tracks at revolute joint A and revolute joint B in Fig. 10, collision tracks with a friction coefficient of 0.01 are most

chaotic, and the collision range is larger, indicating that the motion state is improved in the wake of rise of friction coefficient.

4.3.3 Effects of driving velocity with regard to dynamic response

The part analyzes effects of distinct driving speeds concerning rigid body dynamic response of seven-bar mechanism containing dry friction clearances, considering that there are clearances at both A and B of

Fig. 10 Collision trajectory of shaft

(a) Clearance A
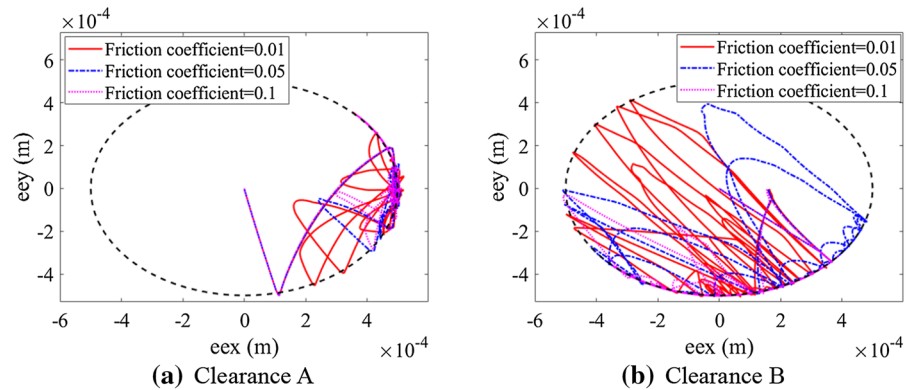
(b) Clearance B

the revolute joints. The driving speeds are chosen for $\omega = \pi$rad/s, $\omega = 1.5\pi$rad/s and $\omega = 2\pi$rad/s. Moreover, clearance figure at A together with B is set as 0.5 mm. Finally, the friction coefficient is 0.01. The displacement, speed as well as acceleration of slider 7 are shown as Fig. 11, concurrently, collision force and collision track at the clearances are revealed as Figs. 12, 13.

In Fig. 11a, the displacement peaks of driving speed $\omega = \pi$rad/s, $\omega = 1.5\pi$rad/s and $\omega = 2\pi$rad/s are 527.1 mm, 527.1 mm and 527.5 mm respectively, indicating in the wake of rise of driving speed, displacement peaks increase, but they are lower than ideal values due to the presence of revolute joint clearances. In Fig. 11b, speed image oscillates at initial position, and then nearly matches the ideal curve. As the driving speed increases, the speed of slider 7 increases accordingly. In Fig. 11c, the acceleration summits of driving speed $\omega = \pi$rad/s, $\omega = 1.5\pi$rad/s and $\omega = 2\pi$rad/s are 592.9 m/s^2, 435.5 m/s^2 and 751.9 m/s^2 respectively, indicating in the wake of rise of driving speed, acceleration image of slider 7 tends to produce more intense vibration and higher peak value in the general trend, especially in the early stage of motion.

It can be seen from the collision diagram at the revolute joint clearance A in Fig. 12a, summits of collision force concerning driving speeds of $\omega = \pi$rad/s, $\omega = 1.5\pi$rad/s and $\omega = 2\pi$rad/s reach 1569 N, 1159 N and 1983 N respectively. Similarly, at clearance B in Fig. 12b, summits of collision force concerning driving speed of $\omega = \pi$rad/s, $\omega = 1.5\pi$rad/s and $\omega = 2\pi$rad/s are 705.8 N, 1403 N and 1902 N respectively. In addition, while driving speeds are $\omega = \pi$rad/s and $\omega = 1.5\pi$rad/s, the

collision force curve only vibrates violently at the beginning of the motion and tends to be stable at the later stage, while when the driving speed increases to $\omega = 2\pi$rad/s, collision force curve always has intermittent vibration. To sum up, the higher the driving speed, the greater the fluctuation range of the collision force at clearances. Furthermore, the higher the peak values of the collision force, the stronger the effects with regard to stability of mechanism.

It can be seen from the collision track images at A and B of the revolute joint clearance in Fig. 13, in the wake of rise of driving speeds, boundary of moving track at clearances is larger, the track is more chaotic, and the collision depth is larger. It can be seen that the larger driving velocity is, the stronger influences on operation stability of mechanism is.

4.3.4 ADAMS simulation verification

For the purpose of checking validity of rigid body dynamic model of 7-bar mechanical containing dry friction clearances, the results obtained by ADAMS virtual simulation software are compared with those in MATLAB. Considering that there are clearances at both A and B of the revolute joints, the clearance values at both A and B of the revolute joints were set to be 0.5 mm, the friction coefficient was selected to be 0.01, and the driving velocity with respect to driving crank 1 and driving crank 4 were chosen to be $\omega=\pi$rad/s. The displacement, velocity and acceleration of slider 7 are shown in Figs. 14, 15, 16.

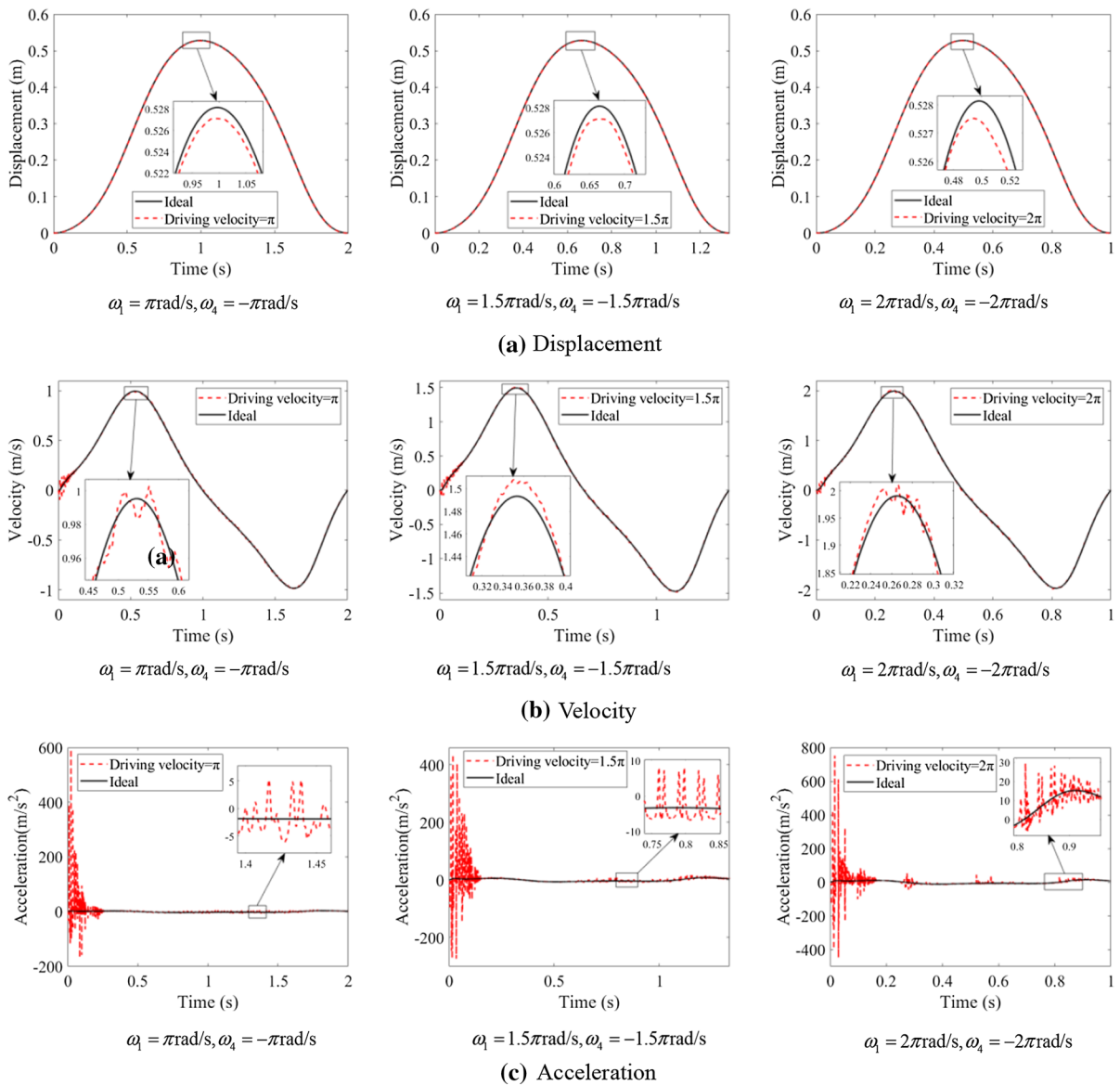According to the displacement image of slider 7 in Fig. 14, the results obtained by MATLAB and

Fig. 11 Dynamic response of mechanism

ADAMS are basically consistent. The image peak value obtained by MATLAB is 0.5271 m, and the image peak value obtained by ADAMS is 0.5292 m. It can be seen from the speed image of slider 7 in Fig. 15 that the speed image fluctuates significantly in the first 0.15 s, and the image obtained by MATLAB fluctuates slightly. In addition, both images produce sawtooth fluctuations at the peak, while the general

trend of velocity images is basically at the same. It can be seen from the acceleration image of slider 5 in Fig. 16 that the acceleration peaks obtained by MAT-LAB and ADAMS occur in 0.0248 s and 0.0128 s respectively, and the peak sizes are 380.7 m/s^2 and 346.5 m/s^2. Both acceleration images fluctuated violently in the first 0.3 s, and then the fluctuation weakened and tended to be stable. Although the time of
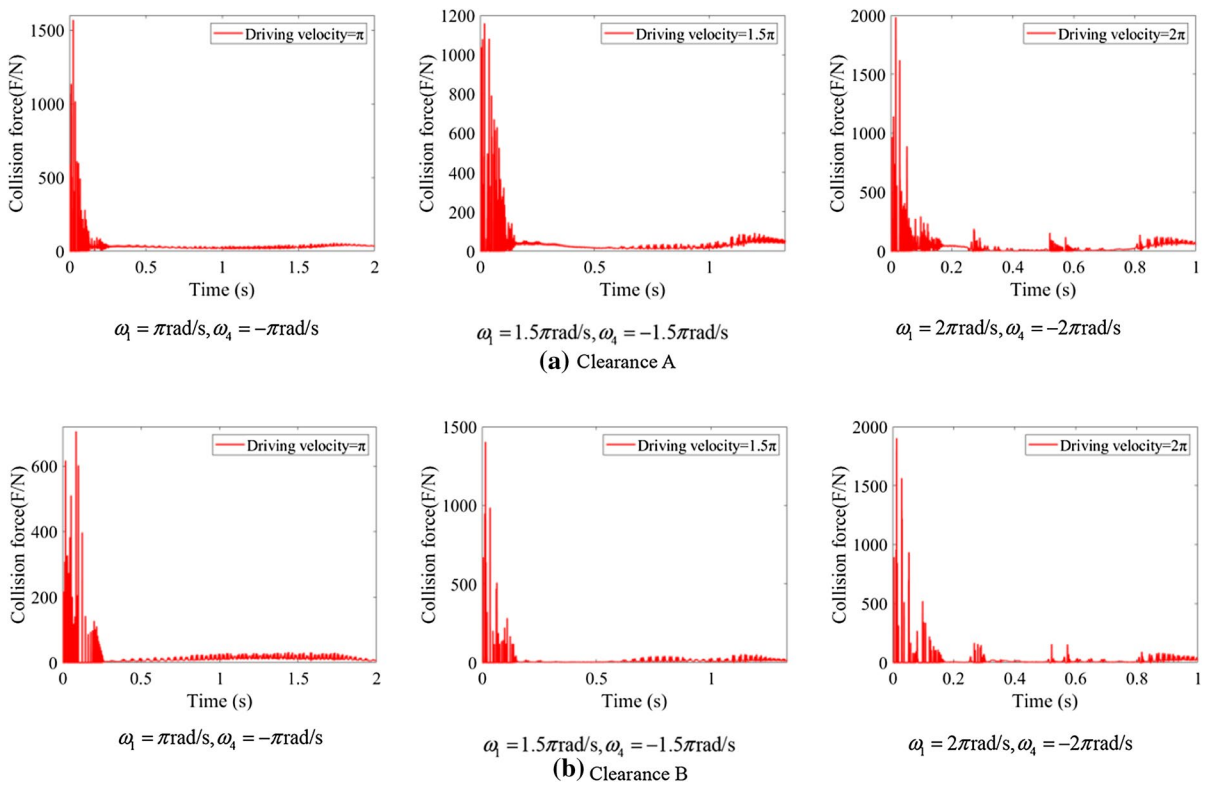
Fig. 12 Collision force at clearance

Fig. 13 Collision trajectory of shaft
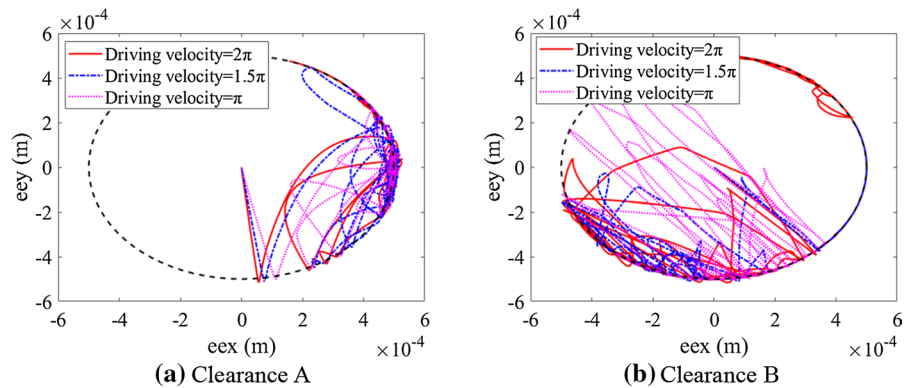
the peak value is slightly offset, the overall trend of the acceleration image remains consistent. The peak error between the two is 34.2 m/s^2, within the allowable error range. To sum up, the comparative analysis results of two different simulation software show that the trend of images obtained by MATLAB and ADAMS software is basically consistent, which verified the correctness of the dynamic model. The reasons for the discrepancy between the results obtained

by MATLAB and ADAMS are the uncertainty of clearance motion simulation, the difference between the two algorithms and solvers, and the diversity in solution accuracy.
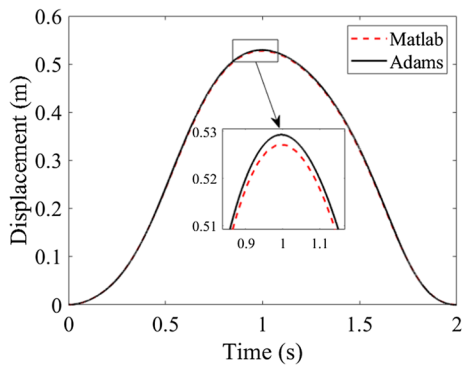
Fig. 14 Displacement of slider 7
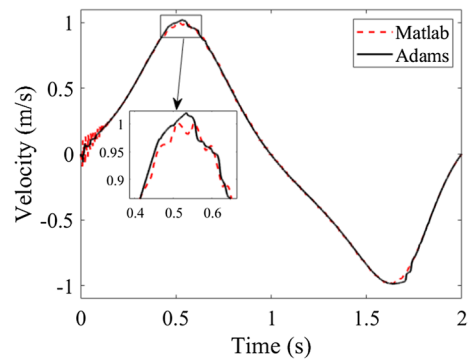
Fig. 15 Velocity of slider 7

5 Analysis on nonlinear characteristics of seven-bar linkage mechanism with dry friction clearances

5.1 Significance of studying nonlinear characteristics

Clearances will cause kinetics concerning mechanism to show some non-linear properties, among which chaos is a common appearance. The study concerning non-linear properties is of vital importance to analyze the influence of clearances with regard to mechanism, and phase diagram as well as Poincare map is significant ways to analyze non-linear properties. Clearance values along with driving speeds are two important
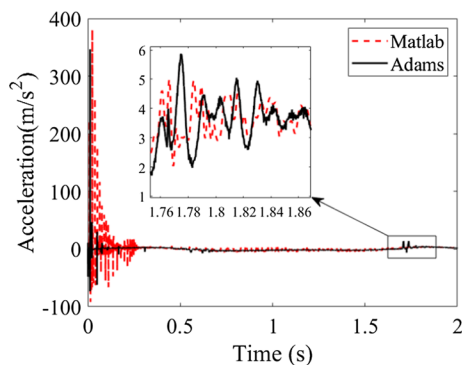
Fig. 16 Acceleration of slider 7

factors affecting the nonlinear characteristics. The nonlinear characteristics of the influencing factors in

a certain interval are analyzed by bifurcation diagram, and the variation rule of the stability is analyzed.

5.2 Effects of clearance values with respect to non-linear properties of multi-link mechanism containing dry friction clearances

This section studied the effects of distinct clearance figure with regard to non-linear properties of 7-bar mechanism with dry friction clearances. Considering that there are clearances at both A and B, the clearance figure of the two revolute joints were both selected to be 0.5 mm and 0.8 mm, and the phase diagram as well as Poincare map in X direction concerning clearances was drawn, as well as the bifurcation diagram changing with the clearance values. Driving velocity was set as $\omega = \pi\,\mathrm{rad/s}$ and friction coefficient as 0.1. The phase diagram along with Poincare map at location A and location B of the revolute joints was shown in Figs. 17, 18, 19, 20, while bifurcation diagram is shown in Figs. 21, 22.

In Fig. 17, at location A, the abscissa range of the phase diagram when the clearance value is 0.5 mm is $[3.887 \times 10^{-4}, 5.022 \times 10^{-4}]$, and the ordinate range is $[-1.098 \times 10^{-2}, 1.102 \times 10^{-2}]$. Most of the Poincare mapping points fit into a closed circle. In Fig. 18, while clearance figure is 0.8 mm, abscissa range of phase diagram in the X direction is $[6.044 \times 10^{-4}, 8.022 \times 10^{-4}]$, and the ordinate range is $[-1.902 \times 10^{-2}, 1.89 \times 10^{-2}]$. Most of the mapping points in the Poincare map are also approximated to a closed circle. According to Figs. 17, 18, the more numerous clearance values, the more extensive scope

Fig. 17 Clearance figure is 0.5 mm at location A

(a) phase diagram **(b)** Poincare map
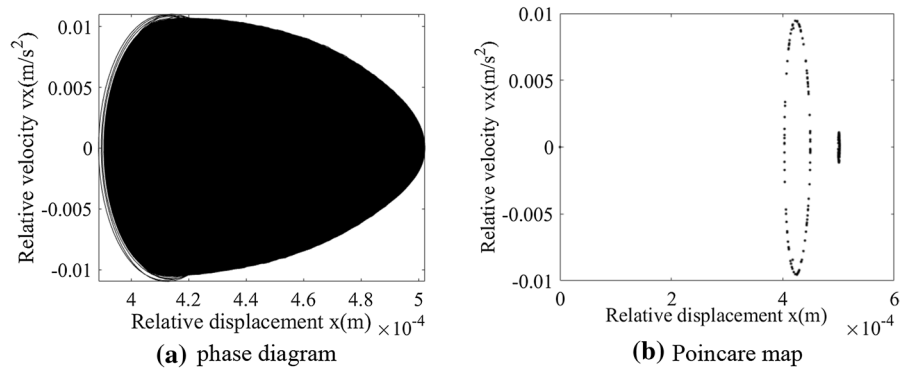
concerning phase diagram and Poincare map, so the mechanism is in quasi-periodic motion state.

In Fig. 19, while clearance figure is 0.5 mm at revolute joint clearance B, the abscissa range of the phase diagram is $[-2.687 \times 10^{-4}, 2.558 \times 10^{-4}]$, and the ordinate range is $[-1.428 \times 10^{-2}, 1.43 \times 10^{-2}]$. In the corresponding Poincare map, Some mapping points are approximated to form a closed circle, while others are more dispersed. As can be seen from Fig. 20, when the clearance value is 0.8 mm at the revolute joint clearance B, the abscissa range of the phase diagram in the X direction is $[-4.603 \times 10^{-4}, 4.332 \times 10^{-4}]$, and the ordinate range is $[-2.586 \times 10^{-2}, 2.457 \times 10^{-2}]$. In the corresponding Poincare map, Some mapping points fit into a closed circle, while others have chaotic and irregular distribution. According to Figs. 19, 20, the larger the clearance value is, the distribution range of points in the phase diagram and Poincare map is larger and more chaotic, and the mechanism is in a state of chaotic motion.

Figures 21, 22 respectively show the bifurcation diagram of the revolute joint clearances at A and B in X and Y orientations in the wake of variety of clearance values. [0.01 mm, 1 mm] is selected as the interval of clearance value. As shown in Fig. 21a, in the wake of rise of clearance values, motion state with regard to revolute joint clearance A in the X direction gradually changes from periodic condition to quasi-periodic motion state. In Fig. 21b, in the interval of [0.01 mm,0.13 mm], the motion of revolute joint clearance A in the Y direction is in quasi-periodic state, while in the interval of [0.13 mm,1 mm], the distribution range of points on the bifurcation diagram gradually expands. At this time, the motion of revolute joint clearance A

in the Y direction is in ataxic condition. Moreover, ataxic condition is increasingly intense. In Fig. 22, in the wake of rise of clearance values, kinematic condition of clearance B in X along with Y orientations gradually ranges from quasi-periodic condition to confused condition. According to Figs. 21, 22, the motion state in the Y direction at location A is most chaotic and has most prominent effects on the stability of system.

5.3 Effects of driving speeds with regard to non-linear properties of 7-bar mechanism with dry friction clearances

The part studied effects of different driving speeds with regard to nonlinear properties of planar 7-bar mechanism with dry friction clearances. Considering that there are clearances at both A and B of the revolute joints, the driving speed was selected as $\omega = 1.5\pi$rad/s together with $\omega = 2.5\pi$rad/s. Furthermore, phase diagram and Poincare map in the X orientation with regard to the clearance were drawn, as well as the bifurcation diagram changing with the driving speeds. Set the clearance value of the two clearances as 0.5 mm and the friction coefficient as 0.1. The phase diagram and Poincare map at location A as well as location B of the revolute joint were shown in Figs. 23, 24, 25, 26, and the bifurcation diagram was revealed as Figs. 27, 28.

In Fig. 23, at location A, while driving velocity is $\omega = 1.5\pi$rad/s, abscissa range concerning phase diagram in the X direction is $[3.564 \times 10^{-4}, 5.028 \times 10^{-4}]$, and the ordinate range is$[-2.176 \times 10^{-2}, 2.201 \times 10^{-2}]$. The distribution of Poincare mapping points is concentrated but irregular. As can be seen from Fig. 24, while

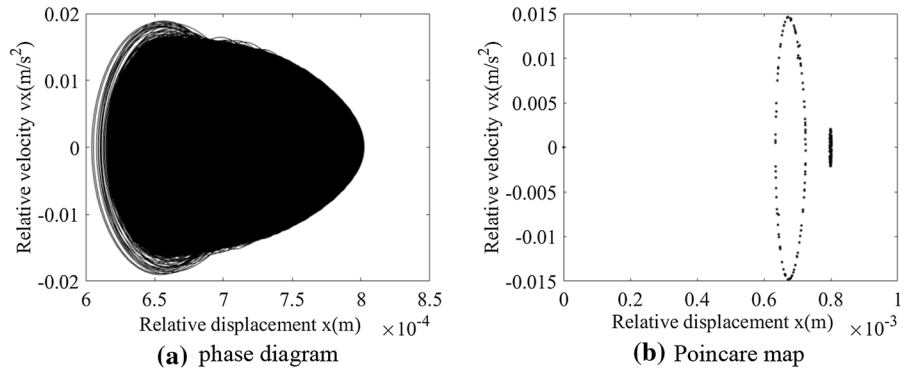**Fig. 18** Clearance figure is 0.8 mm at location A

(a) phase diagram

(b) Poincare map

Fig. 20 Clearance value is 0.8 mm at clearance joint B

(a) phase diagram

(b) Poincare map
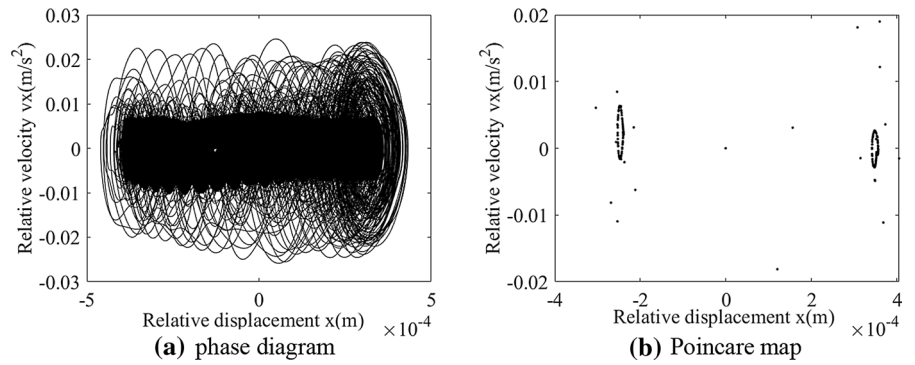
Fig. 19 Clearance value is 0.5 mm at clearance joint B
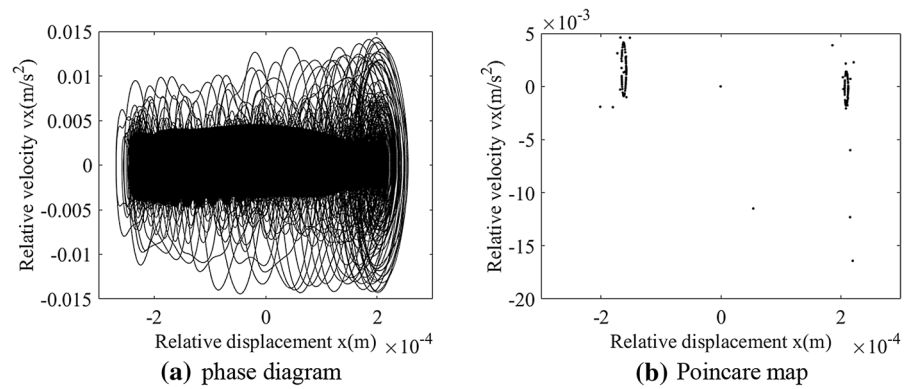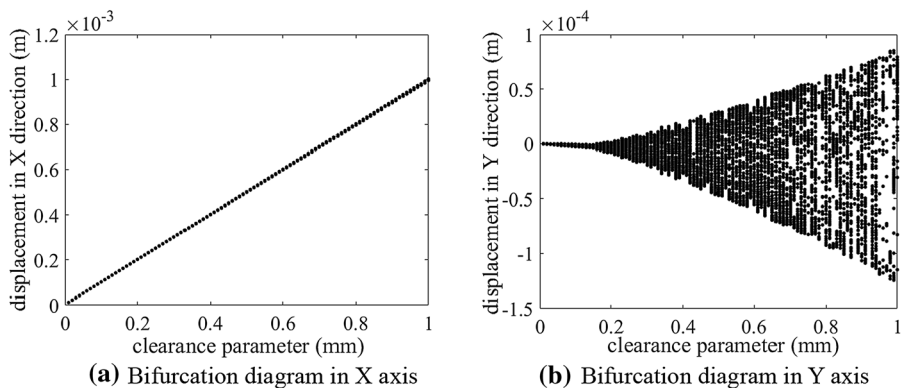
(a) phase diagram

(b) Poincare map

Fig. 21 Bifurcation diagram at clearance A

(a) Bifurcation diagram in X axis

(b) Bifurcation diagram in Y axis

Fig. 22 Bifurcation diagram at clearance B

(a) Bifurcation diagram in X axis

(b) Bifurcation diagram in Y axis

Fig. 23 Driving speed is $\omega = 1.5\pi$rad/s at clearance joint A
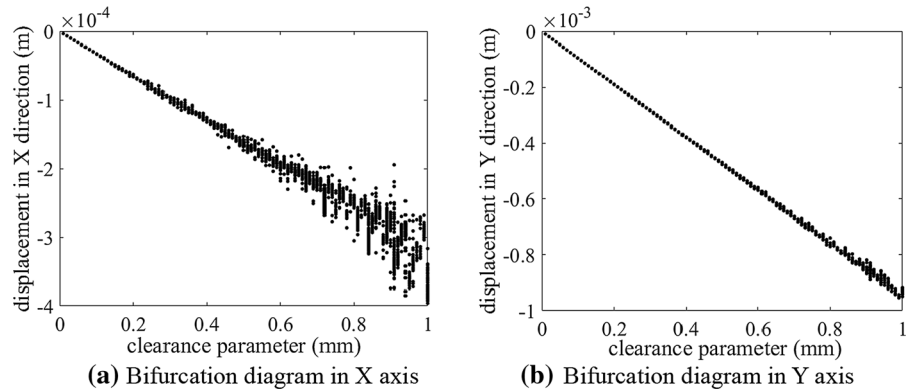
(a) phase diagram
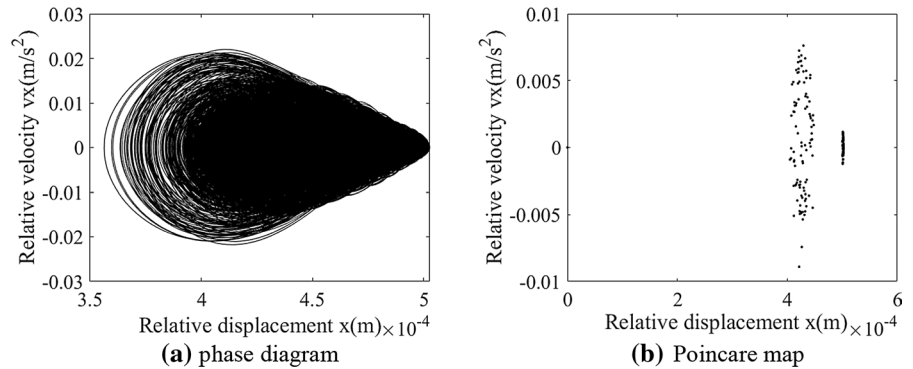
(b) Poincare map

driving velocity is $\omega = 2.5\pi$rad/s, abscissa range concerning phase diagram in the X direction is $[-5.086 \times 10^{-4}, 5.086 \times 10^{-4}]$, and the ordinate range is $[-7.241 \times 10^{-2}, 7.316 \times 10^{-2}]$. The Poincare map has a large distribution range and is in a discrete state. Based on Figs. 23, 24, it can be seen that the driving speed has a large and complex influence on the operation stability of the mechanism, and the mechanism is in chaotic motion.

Figure 25 shows that at revolute joint clearance B, while driving velocity is $\omega = 1.5\pi$rad/s, abscissa range of phase diagram in the X direction is $[-3.799 \times 10^{-4}, 5.004 \times 10^{-4}]$, and the ordinate range is $[-4.696 \times 10^{-2}, 4.599 \times 10^{-2}]$. The mapping points of the Poincare map are mainly distributed in two segments $[-4 \times 10^{-4}, -2 \times 10^{-4}]$ and $[1.5 \times 10^{-4}, 4 \times 10^{-4}]$, which are chaotic and irregular. In Fig. 26, at revolute joint clearance B, while driving velocity is $\omega = 2.5\pi$rad/s, abscissa range concerning phase diagram in the X direction is $[-4.583 \times 10^{-4}, 5.013 \times 10^{-4}]$ and the ordinate range

is $[-0.1782, 0.1602]$. The mapping points of the Poincare map are mainly distributed in two intervals $[-5 \times 10^{-4}, -2.5 \times 10^{-4}]$ and $[1.5 \times 10^{-4}, 4 \times 10^{-4}]$. The mapping points on the first interval are approximately a circle, while the mapping points on the second interval are concentrated and disorderly. According to Figs. 25, 26, compared with the revolute joint clearance A, the driving speeds have a greater influence on the revolute joint clearance B and the situation is more complicated. At this time, the mechanism is in a chaotic motion state.

Figures 27, 28 are bifurcation diagrams with regard to clearances at A and B in X and Y orientation changing in the wake of driving speeds respectively. $[\pi$rad/s,3πrad/s$]$ is selected as the driving speed interval. It can be seen from Fig. 27 that the bifurcation diagrams with regard to clearance A in the X as well as Y directions are divergent, suggesting movement at the clearance A was in a chaotic state. In the wake of rise of driving velocity, diffusion degree of points on the bifurcation diagram varies greatly, but on the

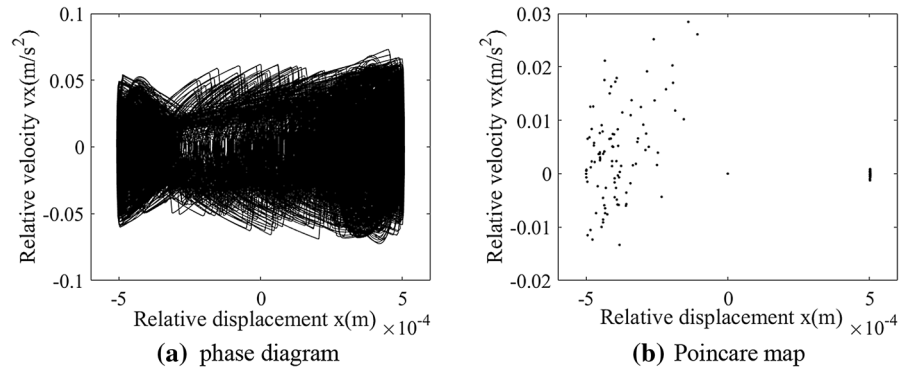**Fig. 24** Driving speed is $\omega = 2.5\pi$rad/s at clearance joint A

(a) phase diagram

(b) Poincare map

Fig. 25 Driving speed is $\omega = 1.5\pi$rad/s at clearance joint B

(a) phase diagram

(b) Poincare map

Fig. 26 Driving speed is $\omega = 2.5\pi$rad/s at clearance joint B

(a) phase diagram

(b) Poincare map

Fig. 27 Bifurcation diagram at clearance A

(a) Bifurcation diagram in X orientation

(b) Bifurcation diagram in Y orientation

Fig. 28 Bifurcation diagram at clearance B

(a) Bifurcation diagram in X orientation   **(b)** Bifurcation diagram in Y orientation
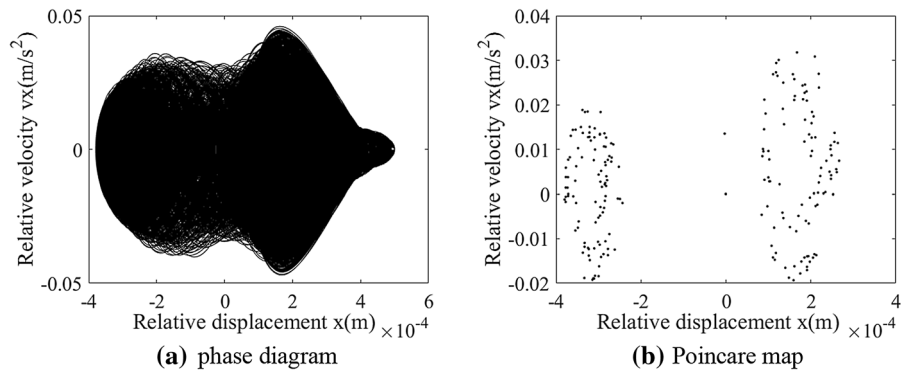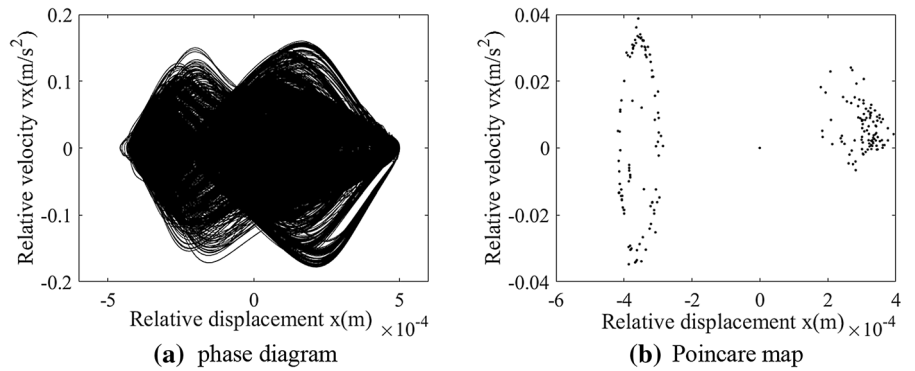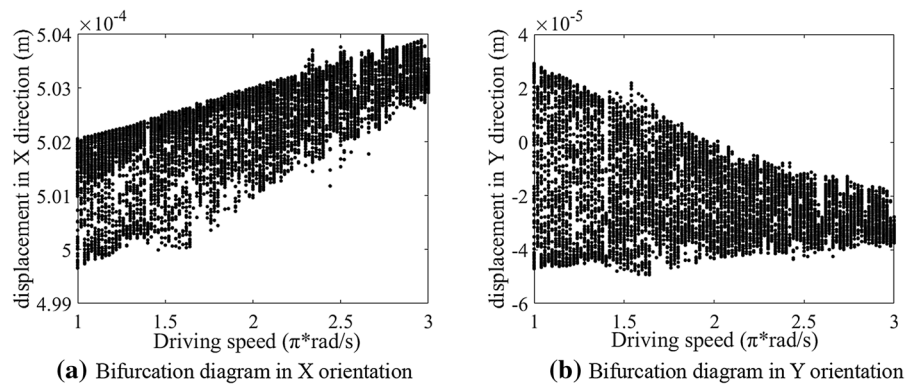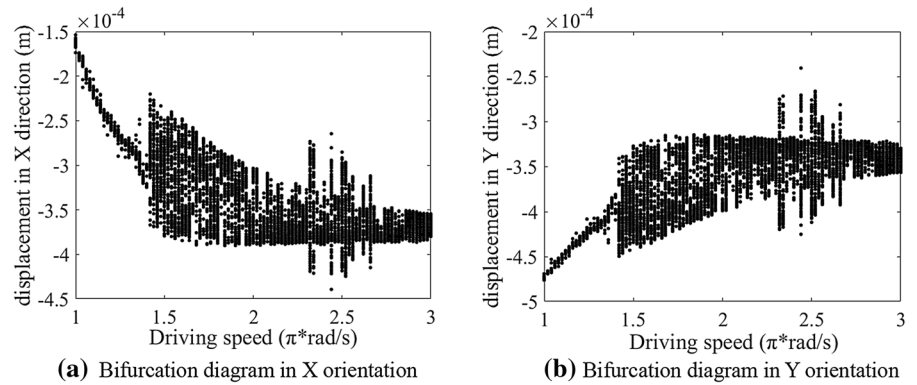
whole, the chaotic state at the clearance A is gradually weakened in the wake of rise of driving velocity. In Fig. 28, while range of driving velocity was [πrad/s ,1.4πrad/s], the points on the bifurcation diagram in the X and Y orientations of clearance B were relatively concentrated, and the motion at the clearance B was in a quasi-periodic state. While driving velocity is $\omega = 1.42\pi$rad/s, distribution range of spots on the bifurcation diagram suddenly expands. When the driving speeds were in [1.42πrad/s,2.3πrad/s], the motion at clearance B was in a confused condition, and confused state gradually weakened in the wake of rise of driving velocity. When the driving speed is in interval of [2.32πrad/s,2.66πrad/s], the distribution range of points on the bifurcation diagram expands again with irregularity. Finally, when the driving speeds were in [2.68πrad/s,3πrad/s], the motion at clearance B returned to quasi-periodic state.

6 Researches on experimental platform of 7-bar mechanism containing double clearances

6.1 Construction with regard to experimental platform

Seven-bar mechanism analyzed in above chapters was laid upright, and its measurement and mass are large, which is not conducive to direct experimental researches. The experimental platform projected in the section laid up each component on a plane and decreases size of every constituent correspondingly, which reduced the manufacturing cost and facilitates the assembly of each component. The two degree of freedom seven-bar mechanism bed-stand was exhibited in Fig. 29, containing rack 5, crank 1, crank 4,

connecting link 2, connecting link 3, connecting link 6, slider 7 and guide rail 8. Aluminum alloy was selected as the material of each component, and its density is 2800 kg/m³. The relative parameters were revealed as Table 4.

6.2 Influences of clearance figures with regard to response of seven-bar mechanism test-bed containing double clearances

In this part, effects of distinct clearance figures concerning test-bed of 7-bar mechanism with double clearances were studied. The driving speed was set as $\omega = 3\pi$rad/s. Moreover, shafts with clearance figures of 0.3 mm as well as 0.6 mm were selected for the experiment. When the mechanism reached a stable state, 21 T ~ 30 T data was selected for analysis. The effects of distinct clearance values with respect to acceleration of slider were exhibited in Fig. 30.

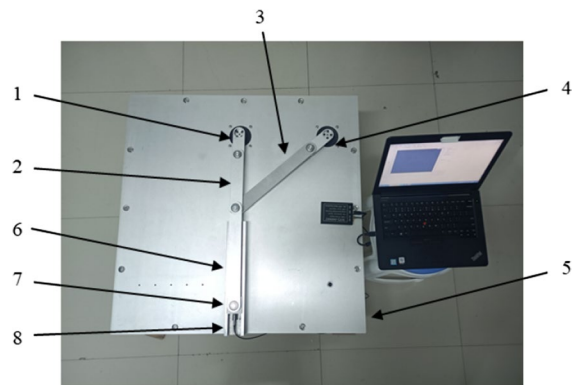In Fig. 30a, the greater the clearance figure, the lower the vibration frequency of the acceleration

Fig. 29 2DOFs 7 bars mechanism test-bed

Table 4 Size and inertia parameters

Components	Length (m)	Mass (kg)	Moment of inertia (10^{-3} kg/m^2)
Crank 1	0.080	0.107	0.118
Connecting link 2	0.180	0.219	0.774
Connecting link 3	0.318	0.374	3.595
Crank 4	0.080	0.107	0.118
Connecting link 6	0.305	0.359	3.200
Slider 7	–	0.139	0.061

Accelerometer was erected at moving orientation with regard to slider to pledge that the acceleration vibrancy semaphore was measured during slider's movement

image of the slider 7, and the larger summits of the vibration. When clearance figure was 0.3 mm, the maximum summit of acceleration was 35.19 m/s^2; while the clearance value was 0.6 mm, the maximum summit was 38.47 m/s^2. This shows that the greater the clearance figure was, the more intense the collision between shaft and bearing was, the lower the

stability of mechanism was and the violent fluctuation of acceleration was.

As is shown in Fig. 30b and c, the consequences in theory of acceleration image were contrasted with experimental consequences. When clearance figure was 0.3 mm, the largest acceleration peaks corresponding to experimental and theoretical consequences were 33.4 m/s^2 and 9.468 m/s^2 separately. While clearance figure was 0.6 mm, maximum acceleration peaks corresponding to the experimental as well as consequences in theory were 35.48 m/s^2 and 10.26 m/s^2 separately. In general, the experimental consequences were basically identical to consequences in theory, and time of vibration peak and the size of vibration peak were deviated. The factors causing the deviation may be the sensitivity error of the accelerometer, the friction effects between slider and track, precision error of test-bed during manufacturing as well as assembly and vibration of the test-bed at high speed. Therefore, the experimental results
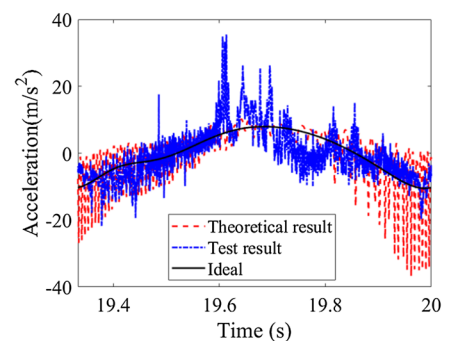

Fig. 30 Effects of distinct clearance values with regard to slider's acceleration when involving double clearances
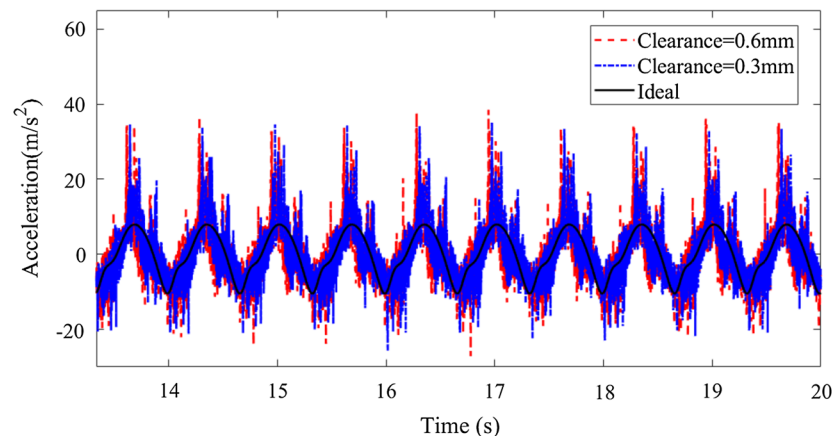
(a) Test results of 10 circles (21T~30T)
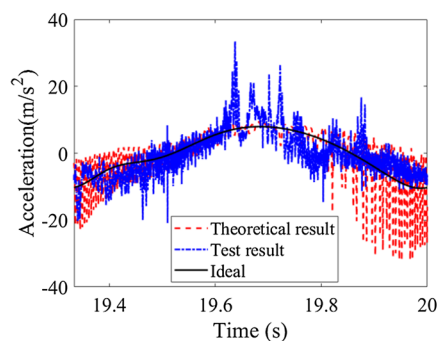
(b) Clearance figure is 0.3mm (30T)

(c) Clearance figure is 0.6mm (30T)

basically verified the correctness of the theoretical results.

6.3 Effects of driving speeds concerning response of seven-bar mechanism test-bed containing double clearances

In the part, effects of distinct driving speeds on test-bed of 7-bar mechanism with clearances were analyzed. Clearance figures with regard to the two rotational joints were put up as 0.6 mm. By adjusting motor speeds, different driving speeds could be obtained at the cranks. Crank 1 and crank 4 with speeds of 60 rpm and 90 rpm were selected for comparison, and the impact of different driving speeds on the acceleration of the slider was analyzed, as shown in Fig. 31.

In Fig. 31a and b, while mechanism operated stably, by analyzing the experimental data from the 21st cycle to the 30th cycle, the larger the driving speed was, the higher the acceleration vibration frequency of the slider 7 was, and the greater the peak value of the vibration was. When the driving speeds of crank 1 together with crank 4 was 60 rpm, the maximum acceleration peak of slider 7 was 21.47 m/s^2; When the driving speeds of crank 1 and crank 4 was 90 rpm, the maximum acceleration of slider 7 was 38.47 m/s^2. This suggests that the faster driving speed was, the higher collision frequency at clearances' interfaces was, which reduced operating performance of mechanism.

In Fig. 31c and d, theoretical results of acceleration image were compared with the experimental results. When the velocity of crank 1 and 4 was 60 rpm, the maximum acceleration peaks corresponding to the experimental and consequences in theory were 18.49 m/s^2 and 4.865 m/s^2 separately. While the speed of crank 1 as well as crank 4 was 90 rpm, the maximum acceleration peaks corresponding to the experimental and consequences in theory were 35.48 m/s^2 and 10.26 m/s^2 separately. In general, the consequences in experiment were basically in accordance with the consequences in theory, and time of vibration peak and the size of vibration peak were deviated. The factors of deviation were consistent with Sect. 6.2.

7 Conclusions

In this article, a nonlinear dynamic analysis framework of multi-link mechanism with dry friction clearances was proposed, by combining theory with experiment, the influence of joint clearances on the dynamic response and nonlinear characteristics of the mechanism is studied respectively, and the nonlinear dynamic characteristics of the mechanism with joint clearances are accurately revealed. A rigid body dynamic model of a planar 7-bar mechanism containing dry friction clearances was built. Moreover, its dynamic response as well as nonlinear characteristics was analyzed. Lagrange multiplier method and Runge–Kutta technique were applied to model and settle a mechanical device with multiple connecting bars containing dry friction clearances. Influences of various parameters on dynamic response of the mechanism were analyzed respectively, and ADAMS was used for simulation verification. The non-linear properties at clearances of kinematic joints for two elements were resolved via drawing various analyzed images. The experimental platform of seven-bar mechanism was built to check the validity of outcomes. The following verdicts can be drawn:

(1) Normal contact force model was established by using the Hertz model improved by Lankarani and Nikravesh, also tangential friction model was established by using improved Coulomb friction model. Dynamic equation of planar 7-bar mechanism containing dry friction clearances was established through Lagrange multiplier technique, in addition, dynamic equation was numerically settled by Runge–Kutta technique.

(2) Influences of clearance values, friction coefficients and driving velocity on dynamic response of mechanism were analyzed, and correctness of model was verified by emulation contrast with ADAMS. With rise of clearance values and driving velocity and decrease of friction coefficient, displacement of the slider has little influence, and the vibration amplitude and peak value of the speed and acceleration of slider rise. Furthermore, the collision force and collision track range at clearances also increase, and the stabilization of mechanical device decreases.

(3) Influences of clearance values and driving velocity on nonlinear properties of mechanism were analyzed. The larger clearance values are, the more chaotic the motion state at the clearance is, and the
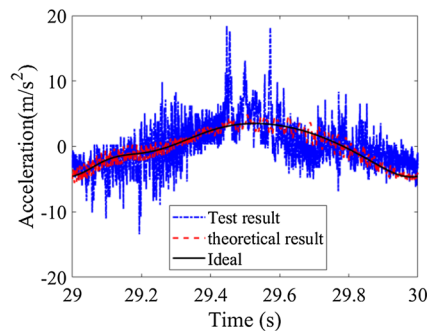
Fig. 31 Effects of distinct driving speeds concerning output terminal acceleration while considering mechanism with double clearances
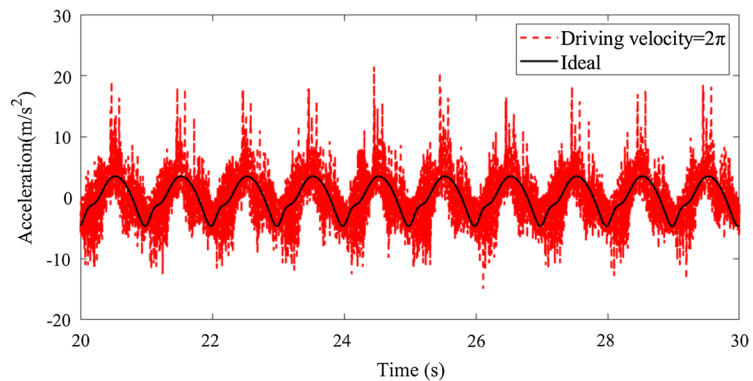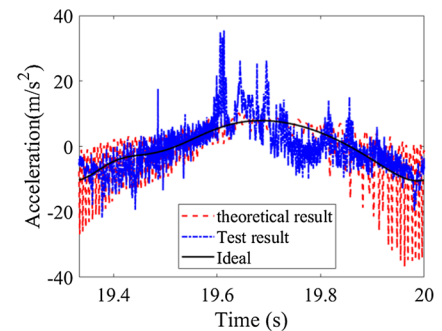

(a) Test results of 10 circles while velocity of crank 1 and 4 are 60rpm (21T~30T)
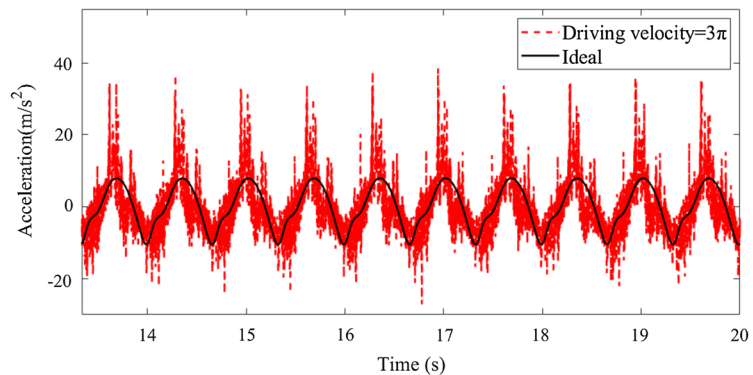
(b) Test results of 10 circles while velocity of crank 1 and 4 are 90 rpm (21T~30T)

(c) velocity of crank 1 and 4 is 60 rpm (30T)

(d) velocity of crank 1 and 4 is 90 rpm (30T)

stronger the chaos phenomenon is, and the stability of the system decreases. However, effects of driving speeds on non-linearity properties at clearances are complex and not strictly negative correlated. On the whole, the higher driving speeds are, confusion degree of motion state at clearances reduces relatively, and the chaotic appearance tends to attenuate correspondingly, and stability of the system increases relatively.

(4) The experimental platform of 2-DOF seven bar mechanism containing double clearances was built and tested. Influences of clearance values and driving speeds on operating characteristics of experimental platform with double clearances were studied respectively, and the test consequences were compared with theoretical consequences. The experimental consequences are basically accordant with consequences in theory, which verified correctness of the theoretical results.

Declarations

Conflict of interest This manuscript has not been published, simultaneously submitted or already accepted for publication elsewhere. All authors have read and approved the manuscript. There is no conflict of interest related to individual authors' commitments and any project support.

References

1. Campione I, Fragassa C, Martini A (2019) Kinematics optimization of the polishing process of large-sized ceramic slabs. Int J Adv Manuf Technol 103(1–4):1325–1336
2. Ma J, Chen GS, Ji L et al (2020) A general methodology to establish the contact force model for complex contacting surfaces. Mech Syst Signal Process 140:106678
3. Chen Y, Feng J, Peng X et al (2021) An approach for dynamic analysis of planar multibody systems with revolute clearance joints. Eng Comput 37(3):2159–2172
4. Etesami G, Felezi ME, Nariman-Zadeh N (2021) Optimal transmission angle and dynamic balancing of slider-crank mechanism with joint clearance using pareto Bi-objective genetic algorithm. J Braz Soc Mech Sci Eng 43(4):185
5. Bai Z, Jiang X, Li F et al (2018) Reducing undesirable vibrations of planar linkage mechanism with joint clearance. J Mech Sci Technol 32(2):559–565
6. Bai Z, Zhao J, Chen J et al (2018) Design optimization of dual-axis driving mechanism for satellite antenna with two planar revolute clearance joints. Acta Astronaut 144:80–89
7. Erkaya S (2018) Experimental investigation of flexible connection and clearance joint effects on the vibration responses of mechanisms. Mech Mach Theory 121:515–529
8. Chen K, Zhang G, Wu R et al (2019) Dynamic analysis of a planar hydraulic rock-breaker mechanism with multiple clearance joints. Shock Vib 2019:4718456
9. Chen X, Jiang S, Deng Y et al (2019) Dynamic modeling and response analysis of a planar rigid-body mechanism with clearance. J Comput Nonlinear Dyn 14(5):051004
10. Marques F, Flores P, Claro JCP et al (2019) Modeling and analysis of friction including rolling effects in multibody dynamics: a review. Multibody SysDyn 45(2):223–244
11. Lai X, He H, Lai Q et al (2017) Computational prediction and experimental validation of revolute joint clearance wear in the low-velocity planar mechanism. Mech Syst Signal Process 85:963–976
12. Oruganti PS, Krak MD, Singh R (2018) Step responses of a torsional system with multiple clearances: study of vibro-impact phenomenon using experimental and computational methods. Mech Syst Signal Process 99:83–106
13. Ambrósio J, Pombo J (2018) A unified formulation for mechanical joints with and without clearances/bushings and/or stops in the framework of multibody systems. Multibody Sys Dyn 42(3):317–345
14. Tan H, Hu Y, Li L (2017) A continuous analysis method of planar rigid-body mechanical systems with two revolute clearance joints. Multibody Sys Dyn 40(4):347–373
15. Song Z, Yang X, Li B et al (2017) Modular dynamic modeling and analysis of planar closed-loop mechanisms with clearance joints and flexible links. Proc Inst Mech Eng Part C J Mech Eng Sci 231(3):522–540
16. Ebrahimi S, Salahshoor E, Moradi S (2017) Vibration performance evaluation of planar flexible multibody systems with joint clearance. J Braz Soc Mech Sci Eng 39(12):4895–4909
17. Wang G, Qi Z, Wang J (2017) A differential approach for modeling revolute clearance joints in planar rigid multibody systems. Multibody Sys Dyn 39(4):311–335
18. Chen Y, Wu K, Wu X et al (2021) Kinematic accuracy and nonlinear dynamics of a flexible slider-crank mechanism with multiple clearance joints. Eur J Mech A Solids 88:104277
19. Erkaya S (2019) Investigation of joint clearance effects on actuator power consumption in mechanical systems. Measurement 134:400–411
20. Jiang S, Chen X (2021) Test study and nonlinear dynamic analysis of planar multi-link mechanism with compound clearances. Eur J Mech A Solids 88:104260
21. Chen X, Jiang S, Wang S et al (2019) Dynamics analysis of planar multi-DOF mechanism with multiple revolute clearances and chaos identification of revolute clearance joints. Multibody Sys Dyn 47(4):317–345
22. Li Y, Wang C, Huang W (2019) Dynamics analysis of planar rigid-flexible coupling deployable solar array system with multiple revolute clearance joints. Mech Syst Signal Process 117:188–209
23. Tan X, Chen G, Sun D et al (2018) Dynamic Analysis of Planar Mechanical Systems With Clearance Joint Based on LuGre Friction Model. J Comput Nonlinear Dyn 13(6):061003
24. Pi T, Zhang Y (2019) Simulation of planar mechanisms with revolute clearance joints using the multipatch based isogeometric analysis. Comput Methods Appl Mech Eng 343:453–489
25. Tan H, Hu Y, Li L (2019) Effect of friction on the dynamic analysis of slider-crank mechanism with clearance joint. Int J Non-Linear Mech 115:20–40
26. Bai Z, Shi X, Wang P (2017) Effects of Body Flexibility on Dynamics of Mechanism with Clearance Joint[M]. Mech Mach Sci 408:1239–1247
27. Wang LiBo, Makis SV et al (2018) Dynamic characteristics of planar linear array deployable structure based on scissor-like element with differently located revolute

clearance joints. Proc Inst Mech Eng Part C J Mech Eng Sci 232(10):1759–1777

28. Varedi-Koulaei SM, Daniali HM, Farajtabar M (2017) The effects of joint clearance on the dynamics of the 3RRR planar parallel manipulator. Robotica 356:1223–1242

29. Chen Y, Feng J, He Q et al (2021) A methodology for dynamic behavior analysis of the slider-crank mechanism considering clearance joint. Int J Nonlinear Sci Numer Simul 22(3–4):373–390

30. Wu X, Sun Y, Wang Y et al (2021) Correlation dimension and bifurcation analysis for the planar slider-crank mechanism with multiple clearance joints. Multibody Sys Dyn 52(1):95–116

31. Liu Y, Wang Q, Xu H (2017) Bifurcations of periodic motion in a three-degree-of-freedom vibro-impact system with clearance. Commun Nonlinear Sci Numer Simul 48:1–17

32. Kong W, Tian Q (2020) Dynamics of fluid-filled space multibody systems considering the microgravity effects. Mech Mach Theory 148:103809

33. Yousuf LS (2019) Experimental and simulation investigation of nonlinear dynamic behavior of a polydyne cam and roller follower mechanism. Mech Syst Signal Process 116:293–309